

1-1-2008

Simulation, system analysis, and optimization of nematic bipolar droplet in polymer dispersed liquid crystal films

Vajiheh Akbarzadeh
Ryerson University

Follow this and additional works at: <http://digitalcommons.ryerson.ca/dissertations>



Part of the [Polymer Science Commons](#)

Recommended Citation

Akbarzadeh, Vajiheh, "Simulation, system analysis, and optimization of nematic bipolar droplet in polymer dispersed liquid crystal films" (2008). *Theses and dissertations*. Paper 649.

381-7
S442
A35
0008

SIMULATION, SYSTEM ANALYSIS, AND OPTIMIZATION OF NEMATIC BIPOLAR DROPLET IN POLYMER DISPERSED LIQUID CRYSTAL FILMS

by

Vajiheh Akbarzadeh

B.Sc., Sharif University of Technology, 2005

A Thesis

presented to Ryerson University

in partial fulfillment of the

requirements for the degree of

Master of Applied Science

in the program of

Chemical Engineering

Toronto, Ontario, Canada, 2008

© Vajiheh Akbarzadeh

Author's Declaration

I hereby declare that I am the sole author of this thesis or dissertation. I authorize Ryerson University to lend this thesis or dissertation to other institutions or individuals for the purpose of scholarly research.

I further authorize Ryerson University to reproduce this thesis or dissertation by photocopying or by other means, in total or in part, at the request of other institutions or individuals for the purpose of scholarly research

Abstract

SIMULATION, SYSTEM ANALYSIS, AND OPTIMIZATION OF NEMATIC BIPOLAR DROPLET IN POLYMER DISPERSED LIQUID CRYSTAL FILMS

Master of Applied Science, 2008

Chemical Engineering, Ryerson University

Polymer dispersed liquid crystal (PDLC) films play an important role in liquid crystal display technology. PDLC films are used in devices such as switchable windows, complex billboards, and flat panel televisions. PDLC films consist of nematic bipolar droplets dispersed randomly in a polymer matrix. In this work, the effect of droplet shape, physical properties, and external field strength is examined on the performance of PDLC films. Finite element method (FEM) and finite difference method (FDM) are used to model a single droplet with external field applied parallel to the droplet axis of symmetry. Results of previous simulations with FEM are reproduced and compared with those with FDM. Genetic algorithm is employed to determine the optimum aspect ratio, and elastic constant ratio for the droplet, and external field strength with respect to minimum energy, response time, and relaxation time.

Acknowledgments

There are many people that have contributed to the successful completion of this work. First of all, I would like to express my sincere gratitude for the diligent assistance of my advisors, Dr. Ali Lohi, Dr. Simant. R. Upreti, and Dr. Philip. K. Chan, in helping me complete my Master's degree. They have shown continued support and provided valuable advice throughout my graduate studies.

I would also like to extend my gratitude for the technical input and guidance of reading committee as well.

I would like to thank my brother, Vahab Akbarzadeh, for his guidance, help and for being a supportive friend.

Most importantly, I would like to thank my husband, Arsalan Safari, for giving me the greatest support, for his love and understanding, and for helping me keep things in perspective.

Dedication

To my mom and dad who supported me with their endless love,

Table of Contents

Author's Declaration.....	II
Abstract.....	III
Acknowledgments.....	IV
Dedication.....	V
Table of Contents.....	VI
List of Tables.....	VIII
List of Figures.....	IX
List of Appendices.....	XI
Nomenclature.....	XII
1. Introduction.....	1
1.1 Liquid Crystals and PDLC Films.....	1
1.1.1 What are Liquid Crystals?.....	1
1.1.2. What are PDLC Films?.....	5
1.2. Objective of this work.....	8
2. Literature review.....	10
2.1. Optical properties of PDLCs.....	11
2.2. Dynamic behavior of nematic droplets in an external field.....	12
3. Methodology.....	18
3.1. Simulation methods.....	18
3.1.1. Mathematical model.....	18
3.1.2. Numerical methods.....	24
3.2 System analysis.....	31
3.3 Optimization.....	33

3.3.1 Optimization algorithm.....	33
3.3.2 Genetic algorithms.....	34
4. Results and Discussion	41
4.1. Simulation	41
4.1.1. Simulation with Finite Element method.....	42
4.1.2 Simulation with Finite Difference method	44
4.1.3 Comparison of FDM and FEM simulation results	46
4.2. System analysis	50
4.2.1. Effect of aspect ratio on response time and relaxation time.....	50
4.2.2 Effect of external field strength on response time and relaxation time	53
4.2.3 Effect of elastic constant ratio on response time and relaxation time	54
4.2.4 Effect of aspect ratio and field strength on sum of response and relaxation time.....	55
4.2.5 Effect of aspect ratio and elastic constants on sum of response and relaxation time ..	57
4.3 Optimization.....	59
4.3.1. Optimization of PDLC films performance	59
4.3.2. Optimization of PDLC films performance (weighted objective functions)	66
5. Conclusions.....	70
6. Recommendation	72
Appendices.....	73
References.....	93

List of Tables

Table1. Comparison of numerical values of $\langle \phi \rangle$ in simulations with FDM and FEM.....	49
Table 2. Optimization results (effect of population size). Loop number is fixed on 200.....	60
Table 3. Optimization results (effect of loop number).population size is fixed on 500.....	61
Table 4. GA parameters for solving optimization problem in PDLC films performance.....	62
Table 5. Optimization results	64
Table 6. Optimization results for weighted J_{M2}	66
Table 7. Analysis of J_1 and J_2	68
Table 8. Optimization results with two objective functions	68

List of Figures

Figure 1. Liquid crystal phase, and liquid and solid phases of matter.....	3
Figure 2. (a) Smectic A, (b) Smectic C liquid crystals.....	4
Figure 3. (a) Cholestric, and (b) Nematic liquid crystals	5
Figure 4. Polymer dispersed liquid crystal film.....	6
Figure 5. Switchable window.....	7
Figure 6. PDLC films in an external field	8
Figure 7. Configuration of droplets	16
Figure 8. Mesh with unequal spaces for z and r axis, used for comparison of FDM and FEM ...	25
Figure 9. Representation of the cross-section of a spherical droplet, and definition of the cylindrical coordinate system	26
Figure 10. Algorithm for solving PDE with FDM and FEM	30
Figure 11. Director configuration according to the surface anchoring strength.....	32
Figure 12. Simulation with FEM.....	43
Figure 13. Simulation with FDM.....	45
Figure 14. Steady state conditions with external field applied parallel to the droplet axis	

of symmetry.....	47
Figure15. Mean magnitude of orientation angle versus time in FDM simulation.....	48
Figure16. Mean magnitude of orientation angle versus time in FEM simulation.....	48
Figure17. Response time versus aspect	51
Figure18. Relaxation time versus aspectratio	51
Figure 19. Response time versus Z_0	53
Figure 20. Relaxation time versus k_{33}/k_{11}	54
Figure 21. J_{MI} for different Z_0	56
Figure 22. J_{MI} for different elastic constant ratios.....	57
Figure 23. Optimum value of Z_0 in 20 runs of optimization program.....	63
Figure 24. Optimum elastic constant ratios in 20 runs of optimization program.....	64
Figure 25. Optimum elastic constant ratios in 20 runs of optimization program.....	64

List of Appendices

Appendix A. Lagrange interpolating polynomial [35]	73
Appendix B. Reproduction of previous simulations by FEM in literature	74
Appendix C. Testing GA with test functions.....	76
Appendix C.1 Testing GA program with Booth function.....	76
Appendix C. 2. Optimization of Beale function.....	82
Appendix C. 3. Optimization of Easom function.....	87

Nomenclature

A	Rate of deformation tensor
a^*	Length of ellipse ($m \times 10^{-6}$)
b^*	Length of ellipse ($m \times 10^{-6}$)
c	Aspect ratio of droplet
f	Residual vector
f_d	Distortion free energy (U / cm^3)
f_m	Magnetic free energy (U / cm^3)
f_s	Surface free energy (U / cm^3)
H	Magnetic field (T)
Jac	Jacobian matrix
J_{Mi}	Multiobjective function
k_{11}^*	Splay elastic constant ($N \times 10^{-11}$)
k_{22}^*	Twist elastic constant ($N \times 10^{-11}$)
k_{33}^*	Bend elastic constant ($N \times 10^{-11}$)
l^i	Length of binary string for each variable
n	Director
N	Angular velocity of director relative to that of fluid
n_p	Refractive index of polymer matrix
p_c	Cross over rate (%)
p_m	Mutation rate (%)
R	Radius of a circle with same area as the ellipse ($m \times 10^{-6}$)
RAND-MAX	Maximum random number generated by random generator,

t_{rlx}	Relaxation time
t_{rsp}	Response time
\mathbf{V}	Velocity field (m / s)
W_0	Surface anchoring constant ($\text{J m}^{-2} \times 10^{-5}$)
Z_0	Zocher number, relative magnitude of magnetic to elastic torques
θ	Angle of magnetic field with respect to vertical axis ($^\circ$)
ϕ	Actual Polar angle ($^\circ$)
γ_1	Rotational viscosity ($\text{Pa s} \times 10^{-3}$)
γ_2	Irotational viscosity ($\text{Pa s} \times 10^{-3}$)
Γ_e	Elastic torque ($\text{N. m} / \text{cm}^3$)
Γ_m	Magnetic torque ($\text{N. m} / \text{cm}^3$)
Γ_v	Viscose torque ($\text{N. m} / \text{cm}^3$)
ϕ_0	Preferred polar angle ($^\circ$)
$\langle \phi \rangle$	Average of absolute angles for all grid points in a droplet ($^\circ$)
$\langle \phi_{st,on} \rangle$	Average of absolute angles in steady state condition with magnetic field on ($^\circ$)
$\langle n_0 \rangle$	Average refractive index of bipolar droplet
n_0	Refractive index of bipolar droplet
$t_{rlx(max)}$	Maximum relaxation time
$t_{rlx(min)}$	Minimum relaxation time
$t_{rsp(max)}$	Maximum response time
$t_{rsp(min)}$	Minimum response time
χ_a	the electric field susceptibility ($\text{N.T}^{-2} \text{m}^{-2}$)

1. Introduction

A brief description of liquid crystals and polymer dispersed liquid crystal films is given in section 1.1. Section 1.2 is about contribution made by this investigator to this field. Section 2 is the literature survey. The method of simulation and optimization is described in section 3, and results are described in section 4. Lastly, conclusions are presented in section 5.

1.1. Liquid Crystals and PDLC Films

1.1.1. What are Liquid Crystals?

Normally, it is expected that matters exist in three phases of solid, liquid, and gas. However, there are some materials which do not meet the necessary requirements of any of these three categories. Liquid crystals are not quite liquid and not quite solid. Physically, they are observed to flow like liquids, but they have some properties of crystalline solids. Liquid crystals can be considered to be crystals which have lost some or all of their positional order (where molecules are arranged in any sort of ordered lattice), while maintaining full orientation order (where molecules are mostly pointing in the same direction). Figure1 is a representation of liquid crystal and two phases of liquid and solid.

There are different liquid crystalline phases and the existence of these different liquid crystalline phases was discovered in 1888 by an Austrian botanist named Friedrich Reinitzer [1]. Although many scientists came across this liquid crystal state earlier from 1850's to 1888, no complete documentation was reported until Friedrich Reinitzer reported his findings on an organic

substance (cholesterol). He observed that upon heating this substance to 145.5 °C a cloudy liquid formed. Further heating to 178.5 °C turned the substance clear, like normal liquids. This phase was described as the liquid crystal phase; this observation was the beginning of research on liquid crystal phase.

There are different types of liquid crystals; Such as smectic, cholestric, and nematic liquid crystals. In a smectic state, in which a number of important structural variations exist (two typical smectic phases are presented in Figure 2), there is more positional order than nematic and cholestric phases. A smectic is a layered structure with the molecules oriented parallel or tilted relative to the normal layer. They are characterized by absence of positional order within the layers; the molecules have some freedom to move within the layers, while them, as in all smectic phases, are much less free to move between layers. These smectics can therefore be said to be stacks of two-dimensional fluids, but they behave as crystalline across the layers. The absence of in-layer order contributes to their high potential for future electro-optic applications.

The two best known of these are smectic A, in which the molecules align perpendicular to the layer planes, and smectic C, where the alignment of the molecules is at some arbitrary angle to the normal.

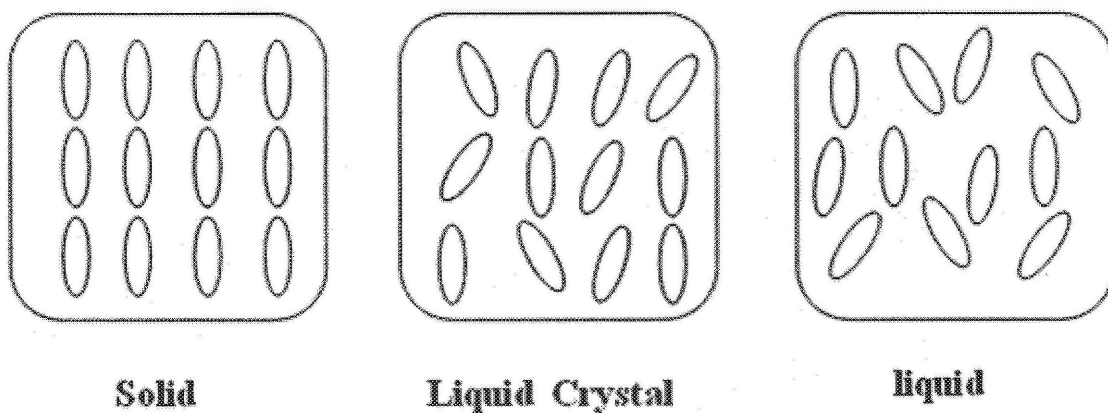


Figure 1. Liquid crystal phase, in between liquid and solid phases of matter.

Another type of liquid crystals is cholesteric liquid crystal which is typically composed of chiral (where the molecules are not similar to their mirror picture) nematic molecules containing a chiral center which produces intermolecular forces that favor alignment between molecules at a slight angle to one another. Figure 3.a shows a picture of cholesteric phase.

Nematics are another type of liquid crystals which are polarizable rod-like organic molecules on the order of 20 Angstroms in length. Nematic comes from a Greek prefix *nemato* meaning threadlike and is used here because the molecules in the liquid align themselves into a threadlike shape. In the nematic phase the molecules are free to move in all directions (i.e. there is no positional order of the centers of mass), but on the average they keep their long axes locally parallel to each other (Figure 3.b). Director is defined as the local average direction of molecules inside the droplet.

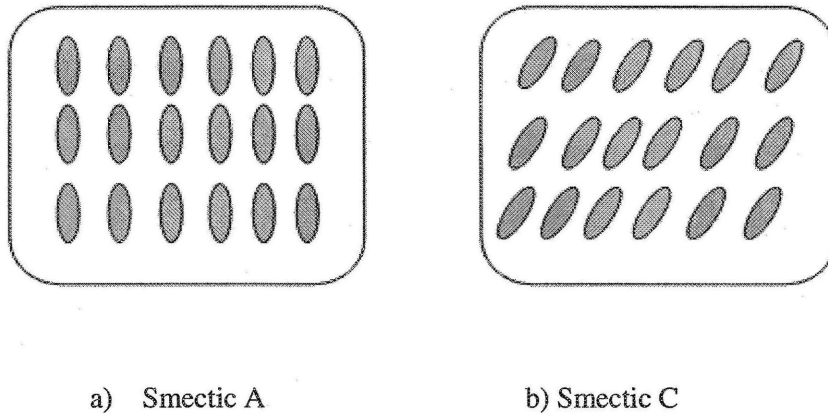


Figure 2. (a) Smectic A, (b) Smectic C liquid crystals.

A nematic liquid crystal is a liquid that causes the polarization of light waves to change as the waves pass through the liquid. The extent of the change in polarization depends on the intensity of an applied electric field. nematic molecules have a tendency to organize themselves in a parallel fashion and their light transmission properties can be deliberately varied as a function of applied external voltage. As a result they demonstrate interesting and useful optical properties. nematic liquids are used in liquid crystal displays (LCDs), such as those found in digital wristwatches and many consumer electronic devices.

A typical nematic liquid crystal produces a 90-degree shift in the polarization of the light passing through when there is no electric field present. When a voltage is applied, an electric field is produced in the liquid, affecting the orientation of the molecules. This causes the polarization shift to be reduced. The effect is slight at low voltages, and increases as the voltage (and the resulting field strength) increases. When the applied voltage reaches a certain level, the polarization shift disappears entirely.

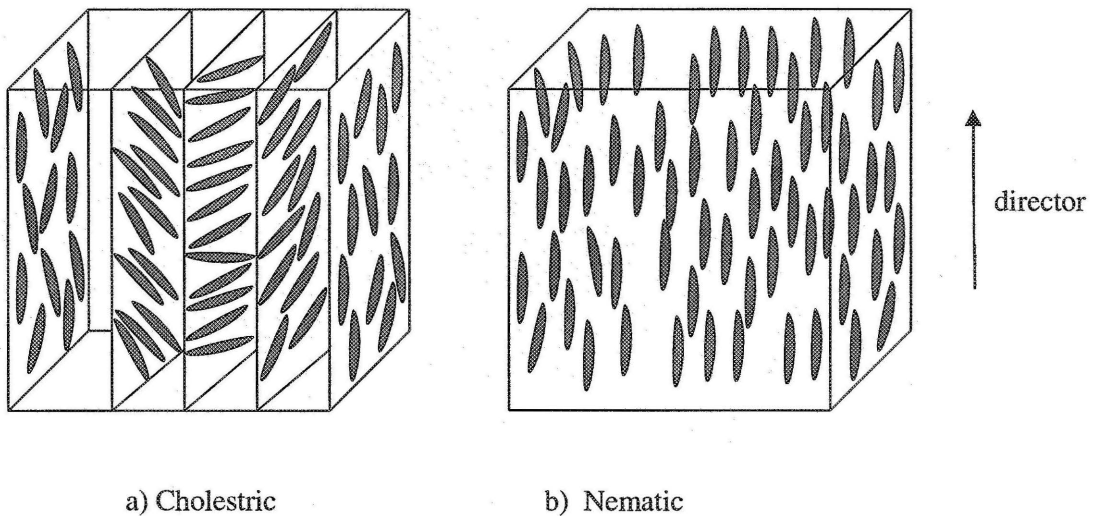


Figure 3. (a) Cholestric, and (b) Nematic liquid crystals

1.1.2. What are PDLC Films?

Polymer dispersed liquid crystal (PDLC) films are relatively new composite materials which have made a revolution in the world of LCD technology, all because of PDLC's excellent electro-optical features. These films consist of low molecular weight bipolar nematic liquid crystals, dispersed in a polymer matrix (Figure 4). Polymer-dispersed liquid crystals are prepared in different ways including: encapsulation (emulsification) and phase separation; the latter process has become the primary method for manufacturing these films. Among the factors influencing the properties of the PDLC material are the shape of the droplet, the types of polymer and liquid crystal used, and cooling and heating rates in production. Different separation methods are thermal induced phase separation (TIPS), polymerization induced phase separation (PIPS), and solvent induced phase separation [3, 4, and 5].

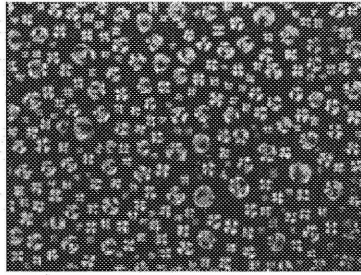


Figure 4. Polymer dispersed liquid crystal film [2]

PDLC films have an interesting characteristic which makes them applicable in electro-optical devices such as billboards and flat panel televisions (Figure 5). These films appear milky white when there is no electric field applied to them due to the refractive index mismatch encountered by incoming light at the liquid crystal/polymer interface. According to Wu et al. [6] the refractive index $\langle n_0 \rangle$ of bipolar droplets in a polymer dispersed liquid crystal film is greater than the refractive index n_0 of a uniform director configuration. So, light is scattered when it is applied to the film and the film appears opaque because: $\langle n_0 \rangle > n_0 = n_p$. Here n_p is the refractive index of polymer matrix. When the external field is applied to the film, $\langle n_0 \rangle$ reduces and approaches $n_0 = n_p$. Right after $\langle n_0 \rangle = n_0 = n_p$ the film becomes transparent and light is no more scattered while passing through the film. Thus, in the on state, if the ordinary refractive index of the liquid crystal within the droplet is sufficiently close to the index of the polymer matrix material ($n_0 \approx n_p$), the incoming light is no longer scattered and the PDLC film becomes clear. When an electric field is applied across the film, the liquid crystal molecules

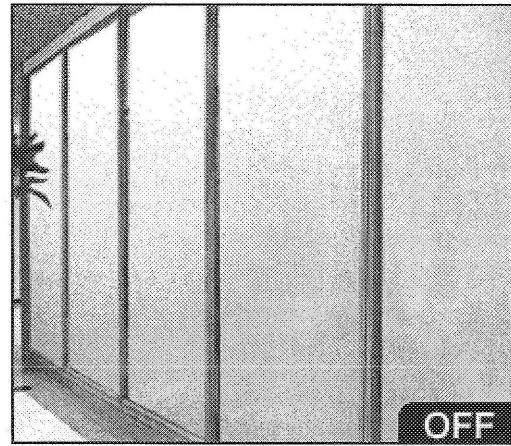


Figure 5. Switchable window; In the left picture external field is on and windows are transparent. On the right field is turned off, result in an opaque window [7].

align with their long-molecular axis parallel to the field direction. In Figure 6 the PDLC film is shown when the electric field is on/off.

The performance criteria for PDLC films are:

- 1) Short relaxation time; after the electric field is switched off, film should go back to its opaque condition fast.
- 2) Short response time; there must be small time interval between the time when electric field is switched on and when the film turns completely transparent.
- 3) Low switching field strength; the film should be efficient and change from opaque to transparent with a low external field.

The performance of PDLC films depend on many factors, such as the initial orientation of the liquid crystals [5], the shape [8], and the size [9] of the droplet.

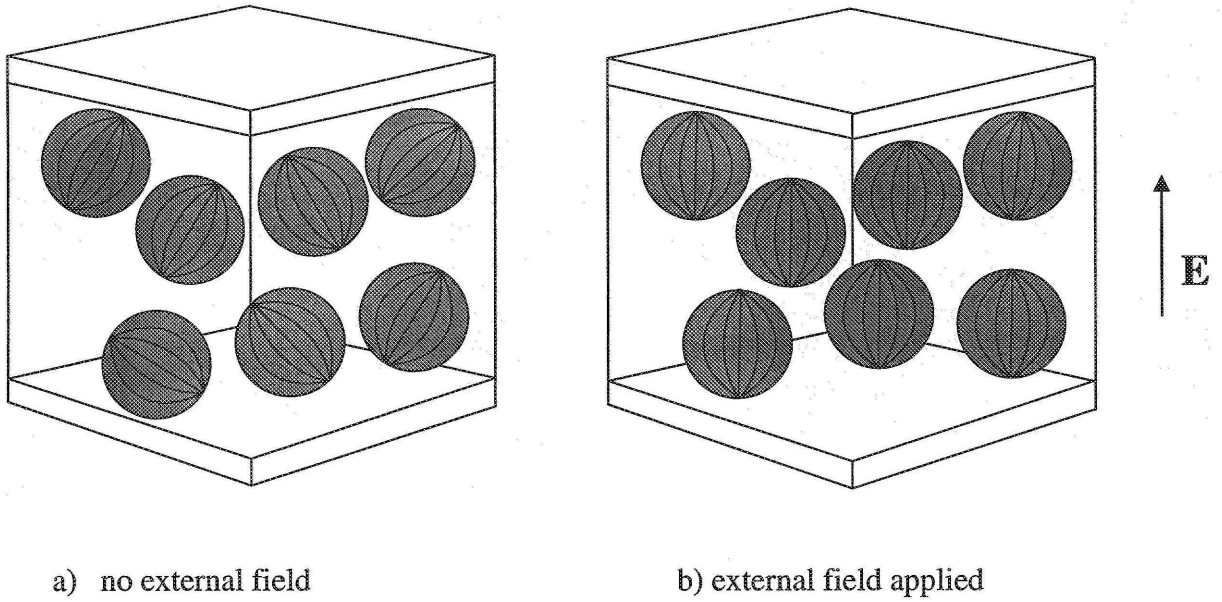


Figure 6. PDLC films in an external field

1.2. Objective of this work

There have been computational and experimental studies on performance of a nematic bipolar droplet in an external field [9, 11, and 32]. In the works by Chan [11] the effect of aspect ratio of a bipolar droplet, and external field strength is studied on relaxation time of nematic droplet. He used finite element method (FEM) for his simulation. Rudhardt et al. [9] have observed the response and relaxation time of a bipolar nematic droplet to an external field. These researchers verified the simulations reported by Chan [11]. Wu et al. [32] have studied the response and relaxation time for a droplet, and operating voltages of light shutters formed from PDLC films. They concluded that in PDLC films with nematic bipolar droplet, aspect ratio is an important

factor in performance of the light shutter. Besides, it has always been interesting to have PDLC films with small field strength to save in energy costs.

The properties of liquid crystal droplet and polymer matrix affect the performance of a PDLC film. In this work, the effect of physical properties of a nematic bipolar droplet is studied on performance of PDLC films. A single droplet is simulated by finite difference method (FDM) because it is a faster method in comparison to previous simulations by FEM. Results of simulation is compared with previous simulation done by Chan [11] for verification. By using genetic algorithm the optimum physical properties of nematic bipolar droplet, and optimum external field strength is defined subject to the constraints of small relaxation time, small response time, and small external field strength. By controlling the temperature and size of molecules used in preparation of PDLC films, it is possible to control the aspect ratio or elastic constant ratio of the nematic droplet in PDLC films.

The model incorporates an external magnetic field to induce director, because the magneto-optical response of PDLC films has the same characteristic properties as the electro-optical response [10]. The external field direction is parallel to the droplet axis of symmetry to minimize the field strength required for reorientation of molecules.

2. Literature review

The first polymer dispersed liquid crystal devices were demonstrated by James Fergason [12]. Fergason together with Schadt and Helfrich invented the twisted nematic liquid crystal display. In the experimental parts, Fergason noted that mixing a nematic liquid crystal with a water-based solution of polyvinylalcohol enabled him to cast a turbid, flexible film. This electro-optical paint was coated onto a plastic sheet, and the plastic sheet was coated with indium-tin oxide (ITO). After drying the film, another sheet of ITO-based film was placed on the other side of film. By applying an AC voltage across the turbid film it became clear, providing a means to a flexible, large area optical shutter. Fergason [12] filed his first U.S. patent in this area in 1981, which was granted in 1984.

Heilmeier [13] was working at David Sarnoff Research Center in 1963 when he and Richard Williams published a report suggesting the use of liquid crystal materials for display. Heilmeier's liquid crystal displays used DSM or dynamic scattering method, wherein an electrical charge was applied which rearranged the molecules so that they scatter light. Heilmeier used the twisted nematic field effect of liquid crystals invented by James Fergason in 1969 and introduced to the market in 1971; Heilmeier is credited with setting the ball in motion for LCDs use in calculators, watches, computers and other instruments. In 1968, he was recognized by RCA with its prestigious David Sarnoff Award.

Doane and Zumer [14] stated that when electric-field is applied to the mixture of an epoxy resin and liquid crystals the scattering effect is cured. This observation led to phase separation methods for making polymer dispersed liquid crystal film from liquid precursor. PDLC films are

fabricated by thermal-induced, polymerization-induced, and shear-induced phase separation methods and also emulsification method [3, 4, and 5].

Besides, Doane and Zummer [14] named 'Polymer Dispersed Liquid Crystals' and 'PDLC' for these materials.

2.1. Optical properties of PDLCs

The interesting optical properties of PDLC films captured the attention of many researchers. Aphonin et al. [15] studied the optical properties of a stretched PDLC film with bipolar nematic droplet.

Zhao et al. [16] investigated the order parameter of a stretched PDLC film as a function of strain by means of in framed dichorism. But he did not consider the effect of polymer orientation surrounding the droplet where Amimori et al.[17] stated that polymer orientation strongly influence liquid crystal molecules at the planar surface and in display applications and optical properties of LCDs.

Amimori et al. [17] studied the Opt-mechanical properties of stretched PDLC films for scattering polarized applications. They have considered the effect of the polymer orientation surrounding the droplet. They also applied Monte Carlo simulation based on the Lebwohl-Lasher model to explain the subtle influence of polymer orientation on liquid crystals.

Higgins et al. [18] studied an individual PDLC droplet and its field-induced dynamics by high-resolution near-field scanning optical microscopy (NSOM) and multiphoton-excited fluorescence microscopy (MPEFMO).

Xie and Higgins [19] studied on Films of nematic LC dispersed in a poly (isobutyl methacrylate) matrix when induced by an electric field applied laterally across each droplet, using two parallel copper wires embedded in the film.

2.2. Dynamic behavior of nematic droplet in an external field

The complex hydrodynamic behavior of a nematic liquid crystalline system can be described by two vector fields depending upon space and time: the director unit vector (n_1, n_2, n_3) describes the local orientation of the mesogenic phase, and the velocity vector (v_1, v_2, v_3) .

Leslie [20] and Ericksen [21] first derived the constitutive equations that described the time evolution of incompressible isothermal nematic fluids, i.e. the nematic hydrodynamic behavior for some defined initial and boundary conditions.

Leslie-Ericksen (LE) equations are widely used in describing the behavior of nematics, especially for the numerical solutions.

Later on, Baleo, et al. [22] used finite element method to numerically solve the LE equations in two dimensions, considering many simplifying assumptions. These researchers described the behavior of anisotropic viscous fluids in Complex geometries including converging and diverging channels, expansion and contraction flows, as well as flow around spherical obstacles

Han and Rey [23] conducted a numerical analysis of LE equations for rectilinear shear flows of a model rigid-rod nematic polymer in low molar mass nematics and nematic liquid crystalline polymers. They simulated the liquid crystal droplet by using Galerkin finite element method

Chan and Rey [24] discussed a synthesis of LE theory and Euler-Lagrange equations for treating the reorientation dynamics in bipolar nematic droplet.

Gomes and Polimeno [25] numerically simulated nematic liquid crystal in a cylindrical sample rotating around its axis at a constant angular velocity and subject to a magnetic field by solving LE equation. They achieved the computational solution of the problem in three dimensions while they considered the influence of initial and boundary conditions.

A series of theoretical studies on the solution of LE equations in 2 dimensions by numerical methods were conducted by Polimeno, et al. [26] assuming that both the director and velocity fields are constrained to lie in a planar section of the sample.

Chan [27] has shown that PDLC films with elongated bipolar droplet axis of symmetry normal to the film plane or parallel to the external field direction results in minimum required switching field strength in the on state and relaxation time in the off state.

On the other hand, Chan [27] stated that the PDLC film should be designed with the bipolar droplet axis of symmetry oriented within the film plane or normal to the external field direction to maximize film contrast between the on and off states.

Chan [27] simulated the behavior of elongated bipolar nematic droplet in an external field, where the field was aligned parallel, and perpendicular to the droplet axis of symmetry. Numerical

results from the solution of Leslie-Ericksen continuum theory described the magnetically induced nematic director reorientation dynamics inside elliptical droplet with strong surface anchoring. He proposed that:

For the case where magnetic field was applied along the droplet axis of symmetry [10]:

- a) The light that passes through the film increase exponentially by increasing the external field, but it saturates with field strength.
- b) The light that passes through the film increase exponentially by increasing the external field, but it saturates with the time in on-state.
- c) The light that passes through the film increases exponentially by increasing the external field, but it saturates with the time in off state.
- d) By increasing the aspect ratio of droplet, switching field strength increases.
- e) By increasing the aspect ratio of droplet, the decay time decreases.

With the external field applied perpendicular to the droplet axis of symmetry [27]:

- a) The light that passes through the film increase exponentially by increasing the external field, but it saturates with field strength.
- b) The light that passes through the film decreases exponentially by increasing the external field, but it saturates with the time in on-state.

In another simulation Chan et al. [11] elicited the effect of elongated nematic bipolar droplet orientation on the performance of polymer dispersed liquid crystal films. The performance

criteria were low switching film strength in the on state, good light contrast between the on and off states, and short relaxation time in the off state. The numerical results from solution of Leslie-Eriksen continuum theory and Frank liquid crystal theories explain the behavior of a PDLC film in an external magnetic field. The aspect ratio was fixed for 1.5 and the external field orientation varied from 0 to 90 degrees, while bipolar droplet axis of symmetry remained fixed.

Rudhardt et al. [9] have visualized the response and relaxation dynamics of bipolar nematic liquid crystal droplet to an external electric field. With strong planner anchoring, upon application of electric field the surface starts to reorient, followed by reorientation of rest of droplet. They stated that there is no critical electric field strength. After removing electric field, elastic forces restored droplet to its original state. They used a typical film of $39\ \mu\text{m}$, which contains single layer of hexagonally shaped droplet of thickness $7\ \mu\text{m}$, enclosed by PVA walls on an $18\ \mu\text{m}$ hexagonal close packed lattice. In their experiments they focused on behavior of a single droplet and their results verified the simulation reported by Chan et al. [11], who has already stated there is no critical electric field strength to start reorienting the director.

There have been a vast number of researches on effects of different boundary conditions on the performance of LCDs. In theory, liquid crystal droplet is under different boundary conditions such as the following conditions proposed by Mirantsev and Romano [28]:

- a) Radial, where the molecules at the surface are oriented normal to the surface of droplet and point toward the center of droplet;
- b) Bipolar, with the molecules at the surface of droplet oriented tangential to the sphere and directed toward the poles. Radial and bipolar boundary conditions are shown in Figure 7.

There are several other boundary conditions investigated for droplet, for example Prishchepa et al. [29] have studied inhomogeneous boundary conditions for nematic droplet with one hemisphere under bipolar boundary conditions and one hemisphere on the radial boundary conditions.

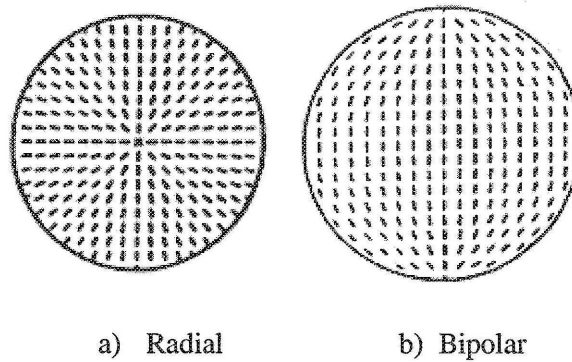


Figure 7. Configuration of droplet [29]

Another critical area of development for PDLC films is reducing the operating voltage for these devices. In these devices, high switching voltage means expensive electronic drivers and reduced operating lifetime for displays. For this reason there is extensive experimental interest in reducing the operating voltage of these devices to 10V or lower.

While Hirai et al. [30] reported of reducing the operating voltage for PDLCs to 6V. There were reports on operating voltage of window prototypes well-over 100V.

Drzaic [31] claimed this difference in the operating voltage is because of different film thicknesses ranging from less than 10 microns to 25 microns or more. Since these are field-effect devices, thicker films require higher voltages.

Doane [8] and Drzaic [3] recognized other criteria for example the droplet size which affects the operating voltage of PDLCs to be the droplet size. They claim that smaller droplet require higher reorientation fields than larger droplet, due to increased curvature of the nematic within small cavities. Also the small-droplet films with higher reorientation voltages often switched faster than lower-voltage films.

Drzaic [3] showed that the nematic droplet size is an important factor in the electro-optic properties of PDLC films, and Drzaic and Muller [4] reported that the droplet shape is equally important to determine the electro-optics of the film. For films using polyvinyl alcohol as the polymeric median the elastic-deformation free energy is minimized when the director field in the droplet is aligned along a major axis of the spheroid; the electric field performs work on the nematic in reorienting the nematic into a higher-energy state. They also estimated the elastic and electric field free-energy-density changes that occur upon reorientation of the nematic droplet.

Recently there have been some experimental studies on the effect of aspect ratio of a nematic bipolar droplet on performance of PDLC films [32]. Wu et al. [32] have studied the response time, the time required for a droplet to reorient completely when the external field is turned on, the decay time, the time required for a droplet to go back to its initial condition after the external field is turned off, and operating voltages of light shutters formed from PDLC's. the bipolar nematic droplet were used with different aspect ratios (1.19 and 1.625). They concluded that in PDLC films with nematic bipolar droplet, aspect ratio is an important factor in the performance of the light shutter.

3. Methodology

This section consists of three parts. First simulation methods are described, in part two criteria for system analysis is explained, and in part three optimization method with genetic algorithm is explained.

3.1. Simulation methods

A brief description of mathematical model is given in section 3.1.1; numerical methods are explained, and algorithm for solving the partial differential equation with finite element method (FEM) and finite difference method (FDM) is presented in section 3.1.2.

3.1.1. Mathematical model

Elliptical model is used to simulate the droplet. The formula is driven from Leslie_ Erickson theory [33]. According to this theory the director reorientation is governed by the following torque balance equation written in Cartesian tensorial notation:

$$\Gamma_e + \Gamma_v + \Gamma_m = 0. \quad (1)$$

where three terms on the left hand side denote the elastic torque, viscous torque and magnetic torque on the director per unit volume, respectively. Their constitutive equations for each are as follows:

$$\Gamma_e = -n \times \frac{\delta f_d}{\delta n} \quad (2)$$

$$\Gamma_v = -n \times (\gamma_1 N + \gamma_2 A \cdot N) \quad (3)$$

$$\Gamma_m = \chi_a (n \cdot H) N \times H \quad (4)$$

The term $\frac{\delta f_d}{\delta n}$ denotes the functional derivative of the distortion free energy density, f_d , with respect to the director n .

The flow of nematics is very much like a flow in conventional organic liquid with molecules of similar size. There have been experimental observations to see if there is any macroscopic displacement of molecules inside a nematic droplet ($V > 0$) when an external magnetic field is applied to the droplet [34] and result is negative. As a result, $V = 0$ in this work and the viscose term in Equation 1 is negligible.

$$N = \dot{n} - \frac{1}{2} [(\nabla V)^T - \nabla V] \cdot n \quad (5)$$

$$A = \frac{1}{2} [(\nabla V)^T + \nabla V] \quad (6)$$

χ_a is electric susceptibility anisotropy, γ_1 is rotational viscosity, γ_2 is irrotational viscosity, N is angular velocity of director relative to that of fluid, A is rate of deformation tensor, n is director, V is velocity field, and H is the magnetic field strength. \dot{n} is the derivative of director with respect to time, and $(\nabla V)^T$ is transpose of matrix ∇V .

In an ideal nematic single crystal, the molecules are (on average) aligned along one common direction n . However, in most practical circumstances, this ideal conformation will not be

compatible with the constraints that are imposed by the external field acting on the molecules. There will be some deformation of the alignment; the deformation may be described by a continuum theory. Equation 7 is the fundamental formula of the continuum theory for nematics and explains the distortion energy inside a droplet.

The total free energy is expressed as follows:

$$F = \int_V f_d dv + \int_V f_m dv + \int_S f_s ds \quad (7)$$

$$f_d = \frac{1}{2} k^*_{11} (\nabla \cdot \mathbf{n})^2 + \frac{1}{2} k^*_{22} (\mathbf{n} \cdot \nabla \times \mathbf{n})^2 + \frac{1}{2} k^*_{33} (\mathbf{n} \times \nabla \times \mathbf{n})^2 \quad (8)$$

$$f_s = \frac{1}{2} W_0 \sin^2(\phi - \phi_0) \quad (9)$$

$$f_m = -\frac{1}{2} \chi_a (\mathbf{n} \cdot \mathbf{H}) \quad (10)$$

The three terms from left to right in Equation 7 are distortion, magnetic and surface free energy densities, respectively. The constants k^*_{11} , k^*_{22} , k^*_{33} are respectively associated with the three basic types of deformation; splay, twist, and bend. It is possible to generate deformation which is pure splay, pure twist, or pure bend. Thus each constant must be positive; dimensions of f_d is an energy (per cm^3 of nematic material). ϕ and ϕ_0 are the actual and preferred orientation angles at the droplet surface. W_0 is the surface anchoring constant.

De Gennes [33] stated that in most practical conditions the surface forces are strong enough to impose a well-defined direction to the director \mathbf{n} at the surface; this is called 'strong anchoring'. In this case instead of minimizing the sum of bulk and surface energies, it is sufficient to minimize only the bulk terms, with fixed boundary conditions for \mathbf{n} .

It is assumed that magnetic field is applied with angle 0 to the droplet axis of symmetry (z axis) in order to minimize the external field required for reorientation of molecules [10]:

$$\mathbf{H} = (H, 0, 0) \quad (11)$$

And the tangential planar two dimensional director field is defined as below:

$$\mathbf{n}(r, z, t) = [\sin(\phi(r, z, t), 0, \cos(\phi(r, z, t))] \quad (12)$$

The following scaling relations are used to non-dimensionalize Equation 1. So, from now on, elastic constant ratios are replaced with their dimensionless values.

$$k_{ii} = \frac{k^*_{ii}}{k} \quad \text{for } i = 1, 2, \text{ and } 3 \quad (13)$$

where $k = \frac{k^*_{11} + k^*_{33}}{2}$, because this simulation is restricted to two dimensions, there is no twist deformation present and $k^*_{22} = 0$.

By non-dimensionalizing r^* , z^* , and t^* , the values of a^* and b^* will be replaced by their dimensionless values as:

$$r = \frac{r^*}{R}, \quad z = \frac{z^*}{R}, \quad a = \frac{a^*}{R}, \quad b = \frac{b^*}{R} \quad (14)$$

$$t = \frac{t^* k}{\gamma_1 R^2} \quad (15)$$

$$Z_o = \frac{\chi_a H^2 R^2}{k} \quad (16)$$

The dimensionless Zocher number, Z_o , gives the relative magnitude of magnetic to elastic torques. The dimensionless time, t , is in order of milliseconds [10].

The equation that explains behavior of orientation angle is derived by solving equations 1-16. The following nonlinear partial differential equation (PDE) describes the magnetically induced director reorientation dynamics [10]:

$$\frac{\partial \phi}{\partial t} = k_1 + k_2 \frac{\partial \phi}{\partial r} + k_3 \frac{\partial \phi}{\partial r} \frac{\partial \phi}{\partial r} + k_4 \frac{\partial^2 \phi}{\partial r^2} + k_5 \frac{\partial \phi}{\partial z} + k_6 \frac{\partial \phi}{\partial z} \frac{\partial \phi}{\partial z} + k_7 \frac{\partial^2 \phi}{\partial z^2} + k_8 \frac{\partial \phi}{\partial z} \frac{\partial \phi}{\partial z} + k_9 \frac{\partial^2 \phi}{\partial z \partial r} - \frac{1}{2} Z_0 \sin(2\phi) \quad (17)$$

Where the constants are:

$$k_1 = -\frac{1}{2} \frac{1}{r^2} k_{11} \sin(2\phi) \quad (18)$$

$$k_2 = \frac{1}{r} (k_{11} \cos^2(\phi) + k_{33} \sin^2(\phi)) \quad (19)$$

$$k_3 = \frac{1}{2} (k_{33} - k_{11}) \sin(2\phi) \quad (20)$$

$$k_4 = k_{11} \cos^2(\phi) + k_{33} \sin^2(\phi) \quad (21)$$

$$k_5 = \frac{1}{2} \frac{1}{r} (k_{33} - k_{11}) \sin(2\phi) \quad (22)$$

$$k_6 = \frac{1}{2} (k_{11} - k_{33}) \sin(2\phi) \quad (23)$$

$$k_7 = k_{11} \sin^2(\phi) + k_{33} \cos^2(\phi) \quad (24)$$

$$k_8 = (k_{33} - k_{11}) \cos(2\phi) \quad (25)$$

$$k_9 = (k_{33} - k_{11}) \sin(2\phi) \quad (26)$$

Boundary and initial conditions:

$$\phi = \phi_0(r, z) \quad \text{at} \quad t = 0, \quad -a \leq r \leq a, \quad -b \leq z \leq b \quad (27)$$

$$\phi = -\tan^{-1}\left(\frac{z}{r}\right) \quad \text{at} \quad t > 0, \quad -a \leq r \leq 0, \quad z = (b^2 - c^2 r^2)^{\frac{1}{2}} \quad (28)$$

$$\phi = -\tan^{-1}\left(\frac{z}{r}\right) \quad \text{at} \quad t > 0, \quad 0 \leq r \leq a, \quad z = (b^2 - c^2 r^2)^{\frac{1}{2}} \quad (29)$$

$$\phi = \frac{\pi}{2} \quad \text{at} \quad t > 0, \quad r = 0, \quad z = \pm b \quad (30)$$

Where c is the aspect ratio and we define it by: $c = b/a$.

The mean magnitude of orientation angle will be defined as below:

$$\langle |\phi| \rangle = \frac{1}{\pi} \int_{-b}^b \int_{-a}^a |\phi| \, dr \, dz \quad (31)$$

By studying the change in mean magnitude of orientation angle, the behavior of molecules in the droplet is defined over the time.

3.1.2. Numerical methods

In this part algorithm of solving Equation 17 with FEM and FDM is described. In section 3.1.2.1, algorithm for solving Equation 17 with FDM is explained. FEM algorithm is described in 3.1.2.2.

It is important to talk about the mesh used for simulation in each section. In the beginning the previous simulations is reproduced with similar mesh used in literature [10]. Second, it is desired to compare the numerical values of orientation angle in each node, in simulation with FDM and FEM to verify applicability of two methods. As a result similar mesh is used in two simulations. Because of FDM sensitivity to mesh near the boundary, it is necessary to have finer spacing in that area and in comparison section an unequal spaced mesh is fine near the boundary with wider spacing in the center of circle. The mesh in literature is equal spaced and it is not fine near the boundary. As a result the following mesh (Figure 8) is used in comparison of two methods. This mesh is unequal spaced. Figure 9 shows the mesh in bipolar configuration and initial condition in the bipolar nematic droplet. Definition for a and b (lengths of the ellipse) is shown in Figure 9. Orientation angle, ϕ , is defined, and θ is the angle of magnetic field with respect to the z axis which is zero in this simulation. Result of mesh refinement with sensitivity of 0.001 indicates that 221 elements is optimum elements for simulation of a single droplet. In system analysis and optimization section, 221 elements is used for simulation of a single droplet.

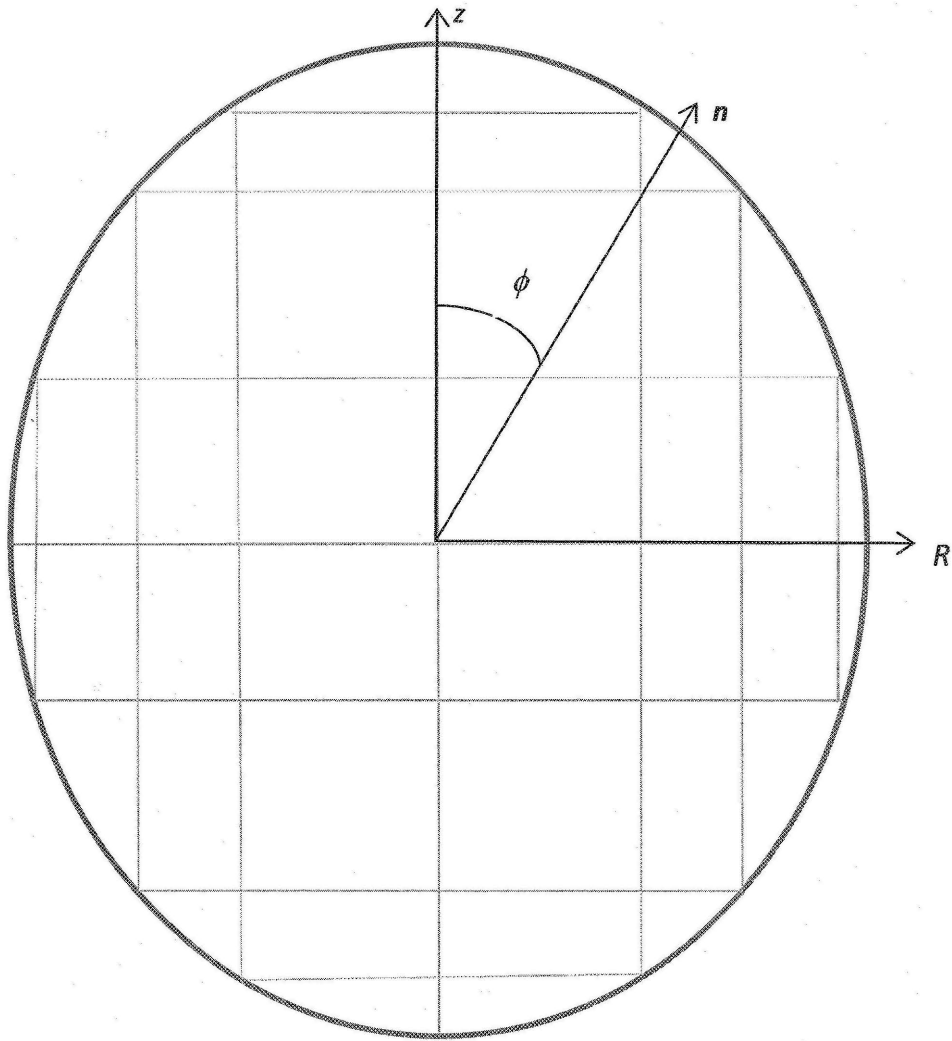


Figure 8. Mesh with unequal spaces for z and r axis, used for comparison of FDM and FEM simulations in section 4.1.3.

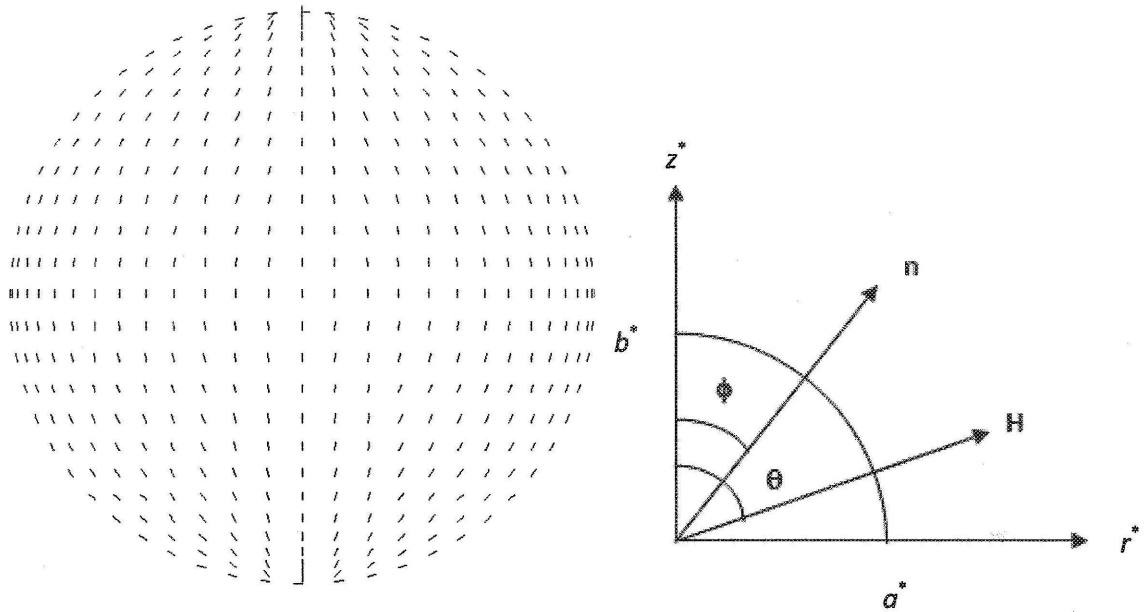


Figure 9. Representation of the cross-section of a spherical droplet, and definition of the cylindrical coordinate system, and the z -axis of symmetry, a^* and b^* are the lengths of the ellipse, ϕ is the reorientation angle of the director n . θ is the angle of magnetic field.

3.1.2.1. Finite Difference Method

Finite difference method (FDM) is one of numerical methods for solving differential equations. In this method the derivatives which appear in the differential equation are replaced by their finite difference approximation [35]. The derivatives can be estimated by two, three, or more number of points. The more number of points used for approximation of derivative, the more improved accuracy of approximation is obtained. There are different methods for approximating the derivatives in PDE [35]. Here the second order lagrange interpolating polynomial is employed to define Equation 17 in finite difference form (Appendix A). The reason for choosing

Lagrange interpolating polynomial is because of its high accuracy in interpolating unequal spaced mesh.

3.1.2.2 Galerkin Finite Element Method [37]

The Galerkin method is a method used for converting a differential equation to a problem of linear algebra or a high dimensional linear system of equations, which may then be projected to a lower dimensional system. These small systems are easier to solve than the original problem, but their solution is only an approximation of the original solution.

Finite element method divides the domain into simply shaped regions or elements. An approximation for the PDE can be developed for each of these elements. The total solution is then generated by linking together or assembling the individual solutions ensuring the continuity at the interelement boundaries. Thus the PDE is satisfied in a piece wise fashion. It should be mentioned that Galerkin Finite element method is one of methods of weighted residuals.

The same mesh and initial condition is used in simulation with FDM and FEM. For time integration fourth order Runge-Kutta method is used with time step of 10^{-4} . The criterion for the steady state condition is the time when the change in $\langle \phi \rangle$ is less than 10^{-5} . Algorithm for solving the PDE with FDM and FEM is shown in Figure 10.

The steps shown in Figure 10 are taken and behavior of $\langle \phi \rangle$ over time is studied. Equation 17 is solved in two dimensions (the mesh is shown in Figure 8). The result of discretizing Equation 17 and derivation of jacobian and residual vectors is presented:

$$Jac.(x^{h+1} - x^h) = -f \quad (32)$$

Jac = jacobian matrix, f = residual vector and by using Gauss elimination method ($x^{h+1} - x^h$), and the values for x vector is defined. Here x represents the right hand side of Equation 17.

$$-f =$$

$$\begin{aligned} det. \left(\int_0^1 \int_0^1 2\pi.k_1.\varphi^i.r + 2\pi.k_2.\frac{\partial\phi}{\partial r}.\varphi^i.r + 2\pi.k_3.\frac{\partial\phi}{\partial r}.\frac{\partial\phi}{\partial r}.\varphi^i.r - 2\pi.\frac{\partial\phi}{\partial r}(\varphi^i.r.\frac{\delta k_4}{\delta r} + \right. \\ \left. k_4.r.\frac{\partial\phi^i}{\partial r} + k_4.\varphi^i) + 2\pi.k_5.\frac{\partial\phi}{\partial z}.\varphi^i.r - 2\pi.k_6.\frac{\partial\phi}{\partial z}.\frac{\partial\phi}{\partial z}.\varphi^i.r - 2\pi.\frac{\partial\phi}{\partial z}(\varphi^i.r.\frac{\delta k_7}{\delta z} + k_7.r.\frac{\partial\phi^i}{\partial z}) + \right. \\ \left. 2\pi.k_8.\frac{\partial\phi}{\partial r}.\frac{\partial\phi}{\partial z}.\varphi^i.r - 0.5.2\pi.\frac{\partial\phi}{\partial z}(\varphi^i.r.\frac{\delta k_9}{\delta r} + k_9.r.\frac{\partial\phi^i}{\partial r} + k_9.\varphi^i) - 0.5.2\pi.\frac{\partial\phi}{\partial r}(\varphi^i.r.\frac{\delta k_9}{\delta z} + \right. \\ \left. k_9.r.\frac{\partial\phi^i}{\partial z}) + 2\pi.k_{10}.\varphi^i.r - 2\pi.\frac{\delta\phi}{\delta t}.\varphi^i.r \right) \quad i, j = 1 \dots n \quad (33) \end{aligned}$$

Definitions of k_1 to k_9 are given in equations 18-26. Definition for k_{10} is given in Equation 35. φ^i is the bilinear basis function used in Galerkin method. det is calculated as:

$$det = \frac{\partial r}{\partial \zeta} \frac{\partial z}{\partial \eta} - \frac{\partial r}{\partial \zeta} \frac{\partial z}{\partial \eta} \quad (34)$$

$$k_{10} = -0.5.Z_o.\sin(2\phi) \quad (35)$$

$$Jac_{ij} =$$

$$\begin{aligned} \int_0^1 \int_0^1 det. \left(2\pi.\frac{\delta k_1}{\delta \phi}.\varphi^i.r + 2\pi.\left(\frac{\partial\phi}{\partial r}.\frac{\delta k_2}{\delta \phi} + k_2.\frac{\partial\phi^j}{\partial r}\right).\varphi^i.r + 2\pi.\left(\frac{\partial\phi}{\partial r}.\frac{\partial\phi}{\partial r}.\frac{\delta k_3}{\delta \phi} + \right. \right. \\ \left. \left. 2.k_3.\frac{\partial\phi}{\partial r}.\frac{\partial\phi^j}{\partial r}\right).\varphi^i.r - 2\pi.\left(\frac{\partial\phi^j}{\partial r}.\left(\varphi^i.r.\frac{\delta k_4}{\delta r} + k_4.r.\frac{\partial\phi^i}{\partial r} + k_4.\varphi^i\right) + \frac{\partial\phi}{\partial r}\left(\varphi^i.r.\frac{\delta^2 k_4}{\delta r^2} + r.\frac{\partial\phi^i}{\partial r}.\frac{\delta k_4}{\delta \phi} + \right. \right. \end{aligned}$$

$$\frac{\delta k_4}{\delta \phi} \cdot \varphi^i) + 2\pi \cdot \left(\frac{\partial \phi}{\partial z} \cdot \frac{\delta k_5}{\delta \phi} + k_5 \cdot \frac{\partial \phi^j}{\partial z} \right) \cdot \varphi^i \cdot r + 2\pi \cdot \left(\frac{\partial \phi}{\partial z} \cdot \frac{\partial \phi}{\partial z} \cdot \frac{\delta k_6}{\delta \phi} + 2 \cdot k_6 \cdot \frac{\partial \phi}{\partial z} \cdot \frac{\partial \phi}{\partial z} \cdot \frac{\partial \phi^j}{\partial z} \right) \cdot \varphi^i \cdot r -$$

$$2\pi \cdot \left(\frac{\partial \phi^j}{\partial z} \left(\varphi^i \cdot r \cdot \frac{\delta k_7}{\delta z} + k_7 \cdot r \cdot \frac{\partial \phi^i}{\partial z} \right) + \frac{\partial \phi}{\partial z} \cdot \left(\varphi^i \cdot r \cdot \frac{\delta^2 k_7}{\delta \phi} + \frac{\delta k_7}{\delta \phi} \cdot r \cdot \frac{\partial \phi^i}{\partial z} \right) \right) + 2\pi \cdot \left(\frac{\partial \phi}{\partial r} \cdot \frac{\partial \phi}{\partial z} \cdot \frac{\delta k_8}{\delta \phi} +$$

$$k_8 \cdot \frac{\partial \phi}{\partial z} \cdot \frac{\partial \phi^j}{\partial r} + k_8 \cdot \frac{\partial \phi}{\partial r} \cdot \frac{\partial \phi^j}{\partial z} \right) \cdot \varphi^i \cdot r -$$

$$0.5 \cdot 2\pi \cdot \left(\frac{\partial \phi^j}{\partial z} \cdot \left(\varphi^i \cdot r \cdot \frac{\delta k_9}{\delta r} + k_9 \cdot r \cdot \frac{\partial \phi^i}{\partial r} + k_9 \cdot \varphi^i \right) + \frac{\partial \phi}{\partial z} \cdot \left(\varphi^i \cdot r \cdot \frac{\delta^2 k_9}{\delta \phi} + r \cdot \frac{\partial \phi^i}{\partial r} \cdot \frac{\delta k_9}{\delta \phi} + \varphi^i \cdot \frac{\delta k_9}{\delta \phi} \right) \right) -$$

$$0.5 \cdot 2\pi \cdot \left(\frac{\partial \phi^j}{\partial r} \cdot \left(\varphi^i \cdot r \cdot \frac{\delta k_9}{\delta z} + k_9 \cdot r \cdot \frac{\partial \phi^i}{\partial z} \right) + \frac{\partial \phi}{\partial r} \cdot \left(\varphi^i \cdot r \cdot \frac{\delta^2 k_9}{\delta \phi} + \frac{\delta k_9}{\delta \phi} \cdot r \cdot \frac{\partial \phi^i}{\partial z} \right) \right) + 2\pi \cdot \frac{\delta k_{10}}{\delta \phi} \cdot \varphi^i \cdot r -$$

$$2\pi \cdot \varphi^i \cdot \varphi^j \cdot \frac{r}{\delta t} \quad i, j=1 \dots n \quad (36)$$

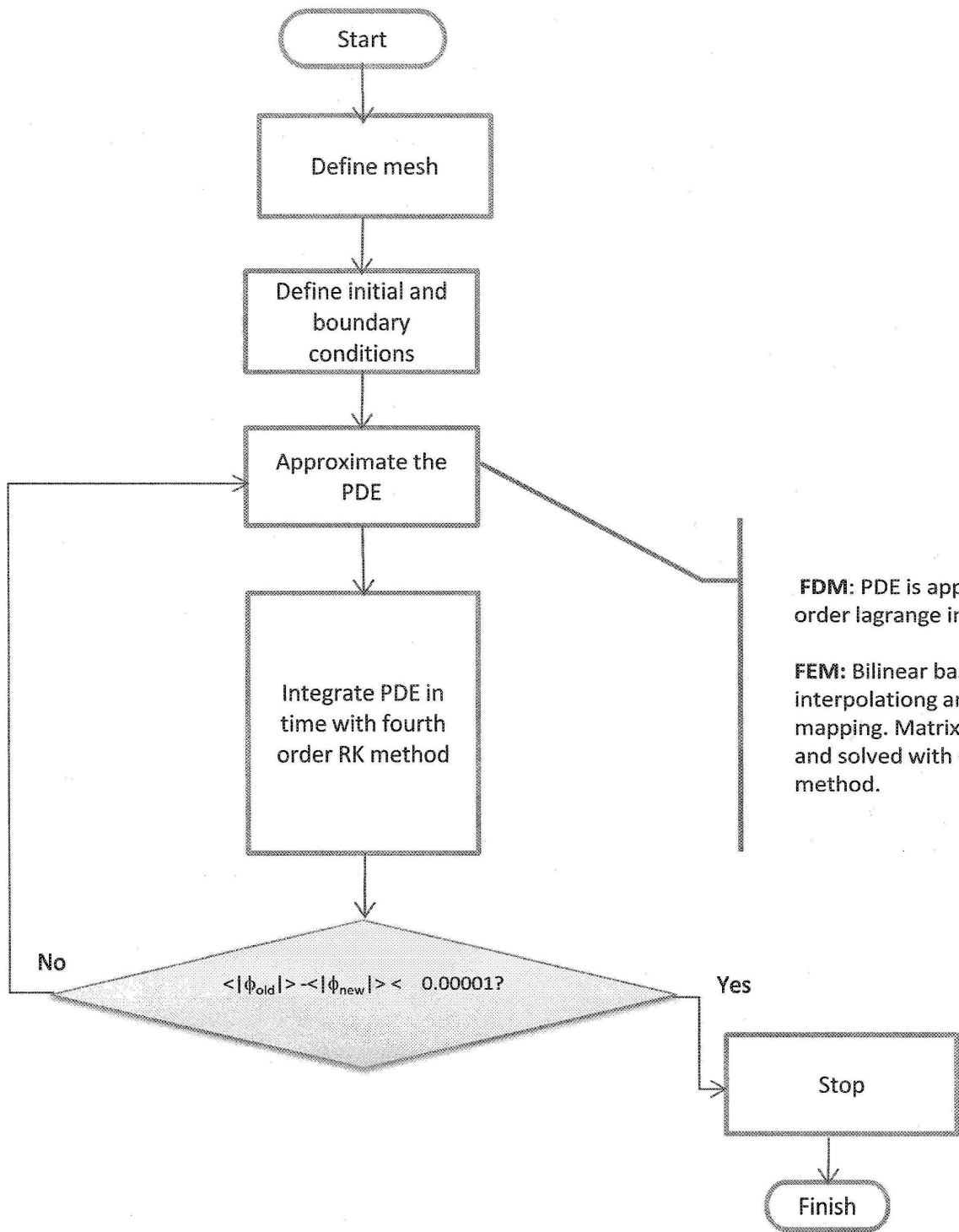


Figure 10. algorithm for solving PDE with FDM and FEM.

3.2 System analysis

In this section, response time (t_{rsp}) and relaxation time (t_{rlx}) are defined. Response time is the time required for bipolar droplet to reorient from initial average orientation angle, $\langle |\phi_0| \rangle$, upon application of an external field, and reach the steady-state condition with magnetic field on, $\langle |\phi_{st.on}| \rangle$. One of the performance criteria for a PDLC film is having minimum response time.

For a droplet to reach to steady state condition, the balance of elastic, viscose, and magnetic torques in Equation 1 should be zero. When the field is turned on, walls (boundary) and magnetic field compete inside the droplet. Because walls play important role in explaining the response time, it is better to first take a look at the constant of anchoring strength, W_0 , which defines how much the external field can reorient the walls. Figure 11 represents three values for W_0 . It is observed that $W_0 = 10^3$ is strong enough to make a bipolar configuration, and result in strong anchoring [24]. In this work, the value of W_0 is 10^3 . So, walls are fixed and do not reorient with external field.

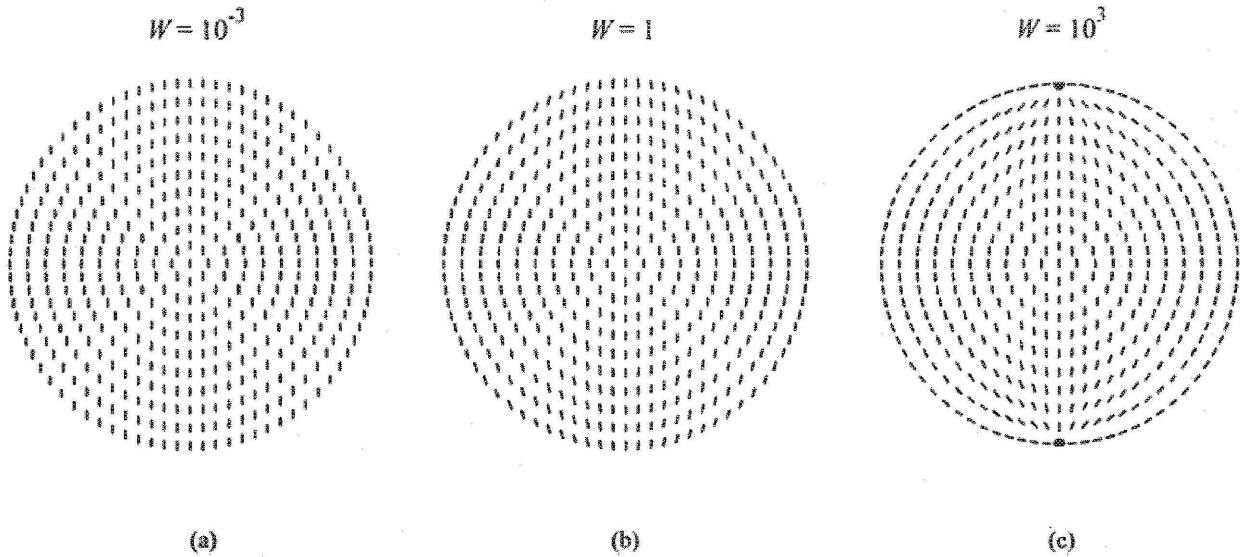


Figure 11. Steady-state director configuration according to the dimensionless surface anchoring strengths: (a) $W=10^{-3}$, (b) $W=1$, and (c) $W=10^3$ [24].

When the field is removed, the orientation of the droplet director returns from an angle of $\langle |\phi_{st.on}| \rangle$ to $\langle |\phi_0| \rangle$. The relaxation time is achieved when the balance of elastic and viscous torques in Equation 1 becomes zero. After the orientation of director reaches $\langle |\phi_{st.on}| \rangle$ field is turned off and the relaxation time is measured.

The three independent variables in a liquid crystal droplet are aspect ratio (c), elastic constant ratio (k_{33}/k_{11}), and magnetic field strength (Z_0). The effect of these variables on the response and relaxation time is studied and presented in sections 4.2.1-4.2.5.

3.3 Optimization

The term optimization refers to the study of problems in which one seeks to minimize or maximize a real function by systematically choosing the values of variables from within an allowed set. This allowed set defines the constraints of the optimization problem.

Here genetic algorithm is used to find optimum aspect ratio (c) of droplet, elastic constant ratio (k_{33}/k_{11}) of molecules inside the droplet, and external field strength (Z_0) subject to the constraints of minimum energy used for reorientation of molecules, minimum time required for reorientation of director in on-state and minimum relaxation time for reorientation of the director in off state. Brief description of genetic algorithm is followed.

3.3.1 Optimization Algorithm

There exists number of optimization algorithms which are mainly divided in two parts of traditional and nontraditional optimization algorithms. There are many traditional methods designed for special optimization problems, such as single-variable optimization algorithms, multi-variable optimization algorithms or constrained optimization algorithms. These algorithms are being used in engineering design problems since sixties, and because of their existence and use for quite some years; they are called traditional optimization algorithms [38].

Nontraditional optimization methods are relatively new methods and are becoming popular in engineering design optimization problems in the recent past. Genetic Algorithms is one of these nontraditional methods.

The advantages of genetic algorithms on traditional methods are:

- 1) None of traditional optimization algorithms are guaranteed to find the global optimum of the objective function. Where genetic algorithm is found to be a better global searcher.
- 2) Sometimes there is more than one global optimum in an optimization problem, and it is necessary to know all the optimum solutions. By using traditional methods we need to apply the method a number of times, and each time start from a different initial solution. This way hopefully one will find a different optimal solution. Genetic algorithms find multiple solutions simultaneously in a single search.

The basic mechanism of a GA is so robust that, within fairly wide margins, parameter settings are not critical. Among nontraditional optimization methods, GA is famous for being a robust global searcher.

3.3.2 Genetic Algorithms

Genetic algorithms are computerized search and optimization algorithms, which are based on the mechanics of natural genetics and natural selection. Professor John Holland of university

of Michigan, Ann Arbor, envisaged the concept of these algorithms in the mid-sixties and published his work [38]. After that many of his students continued working on GAs where the results are published in many papers and books, i.e. [39].

3.3.2.1 Principles of working with genetic algorithms

An optimization problem consists of objective function which we would like to minimize or maximize, $fi(u)$, subject to some constraints which are known from the natural conditions of problem.

Because genetic algorithms are based on selection of the fittest principle of nature to make a search process, the optimization problem should come in the form of maximization. So, the minimization objective function will be changed to a maximization problem with a fitness function. The fitness function has the same optimum as the objective function but in the form of a maximum. A number of such transformations are possible but the most common fitness function is:

$$fitness(u) = \frac{1}{1+fi(u)} \quad (37)$$

First step in solving an optimization problem with GAs is coding the variables. Binary-coded strings having 1's and 0's are mostly used. Each variable is coded with one string S_i with

length l_i . The length of strings can be different from each other. For example if an optimization problem has two variables and are variables are coded with 5 bit strings, the lower and upper limits are presented by (00000 00000) and (11111 11111), because the substrings (00000) and (11111) have the minimum and maximum decoded values. Any other set of 5 bit binary strings represents a point in the search space. The value of each point can be calculated with the following linear function:

$$u_i = u_i^l + \frac{u_i^m - u_i^l}{RAND_MAX - 1} \cdot \text{decoded value of } S_i \quad (38)$$

The decoded value of each string (S_i) is calculated as:

$$\sum_{i=0}^{l-1} 2^i (S_i) \quad (39)$$

Where string S_i is represented as ($S_{l-1} S_{l-2} \dots S_2 S_1 S_0$). It is clear that by increasing the string length l_i by one, the accuracy of answers increases exponentially. The length of each string depends on the desired accuracy of the variable it stands for.

The operation of GAs starts with selecting a population of random strings, representing design variables. After that decoded value of each variable is calculated, and by using the mapping function, the value of variable is found.

Thereafter, each variable is evaluated to find the fitness value. The population is then operated by three main operators- reproduction, crossover, and mutation- to create a new

population of points. Each time a population is gone through these three operators is called a generation.

3.3.2.2 GA Operators

1) Reproduction is the first operator applied on a population. By calculating the fitness value of each string, the good strings are selected and copied in the mating pool with a probability proportionate to their fitness value. Since the population size is usually kept fixed in SGA (simple genetic algorithm), the sum of the probability of each string being selected for the mating pool must be one.

Reproduction operator is sometimes called selecting operator, too. Its working principle is similar to a roulette-wheel with its circumference marked for each string proportionate to the string's fitness. So, a string with small fitness value has smaller probability to be copied in the mating pool.

2) Crossover operator is mostly the second operator applied on a population. In reproduction phase no new strings are formed. And only strings with high probability are copied in the mating pool.

In crossover phase, a coin is flipped with a probability P_c , for two random strings and if the result of flipping the coin is positive, the two strings crossover each other from the

right side of a random bit. For example, when the first two strings from the top of the list in population are (001110001) and (100110101), and imagine that result of flipping the coin was positive, then a random number between 0 and 8 is chosen. Let's imagine that the random number was 4. Now the two strings crossover each other from the right side of the 4th bit, and the result would be:

(001110101) and (100110001)

It can be noticed that the result of crossover is forming new strings. Although crossover is not guaranteed to make good strings but it is not a problem, because if the result of crossover is bad the string does not survive long in the reproduction phase.

- 3) Mutation operator is also responsible to make new strings but it completes the crossover phase. Let's imagine a population as:

00111

01010

01011

00011

Suppose the optimum value has 1 in the left-most bit position. As we noted reproduction operator does not change the strings, so we can't be hopeful to get 1 in that position through reproduction. Besides, the probability of the left-most bit position being changed

in the crossover is much less than the right-most bit. But the mutation operator gives the left-most bit some chance through the probability P_m of turning 0 into 1.

All these three operators work together to hopefully create better strings. Reproduction operator copies the strings with above average fitness values in the mating pool. Then crossover recombines two of the strings in the mating pool to create new substrings. The mutation operator changes a string locally to hopefully create a better string.

Although, none of these steps are guaranteed to create good strings, but as bad strings will be eliminated by the reproduction operator in next generation and good strings will be emphasized. The algorithm for solving an optimization problem with SGA is followed:

3.3.2.3 Algorithm [38]

- Step 1 choose a coding to represent problem parameters, a selection operator, a crossover operator, and a mutation operator. Choose population size, crossover probability P_c and mutation probability P_m . Initialize a random population of strings of size l_i . Choose a maximum allowable generation number.
- Step 2 evaluate each string in the population.
- Step 3 if generation number > maximum allowable generation number, Terminate.

- Step 4 perform reproduction on the population.
- Step 5 perform crossover on random pairs of strings
- Step 6 perform mutation on every string.
- Step 7 evaluate strings in the new population. Set $loop = loop + 1$ and go to step 3.

4. Results and Discussion

In section 4.1, results of simulations are presented. After verifying FDM simulation results system analysis is carried out based on FDM simulation, and presented in 4.2. Multi-Objective optimization results with Genetic Algorithm are described in 4.3.

4.1. Simulation

The main interest of this part is to model behavior of a single bipolar droplet, and study the dynamic behavior of this single droplet when an external field is applied parallel to its axis of symmetry. This section presents numerical results obtained from solving Equation 17 with two numerical methods of FDM and FEM. Simulation results reported by Chan [10] using FEM is reproduced in section 4.1.1, and results obtained with FDM is presented in section 4.1.2. In section 4.1.3 simulation results with FEM and FDM are compared.

The value for elastic constants ($k_{11} = 0.6667$ and $k_{33} = 1.3333$) in Equation 17 are same as the simulations by Chan [10] in this section.

The external field is turned on and behavior of $\langle |\phi| \rangle$ is studied. The time required for the director to reach steady state condition when magnetic field is on, $\langle |\phi_{st.on}| \rangle$, is measured and then the external field is turned off and the relaxation time, the time required for a droplet to reach steady state condition in off state, is measured, too.

4.1.1. Simulation with Finite Element method

Result of simulation with FEM is described in this section. Mesh with 400 elements is used to be consistent with the previous work [10]. Orientation of molecules in their initial condition and after application of an external field ($Z_0 = 2000$ to be consistent with previous simulation [10]) to the droplet is shown in Figure 12. This figure shows the change in director orientation inside a droplet before 12 (a), and after 12(b) external field is applied to it. Upon application of external field all molecules inside the droplet align with the field. $c = 1$ represents a spherical droplet.

It is observed that results of simulation are identical with previous simulations [10]. There is more reproduction of simulations reported by Chan [11] in Appendix B.

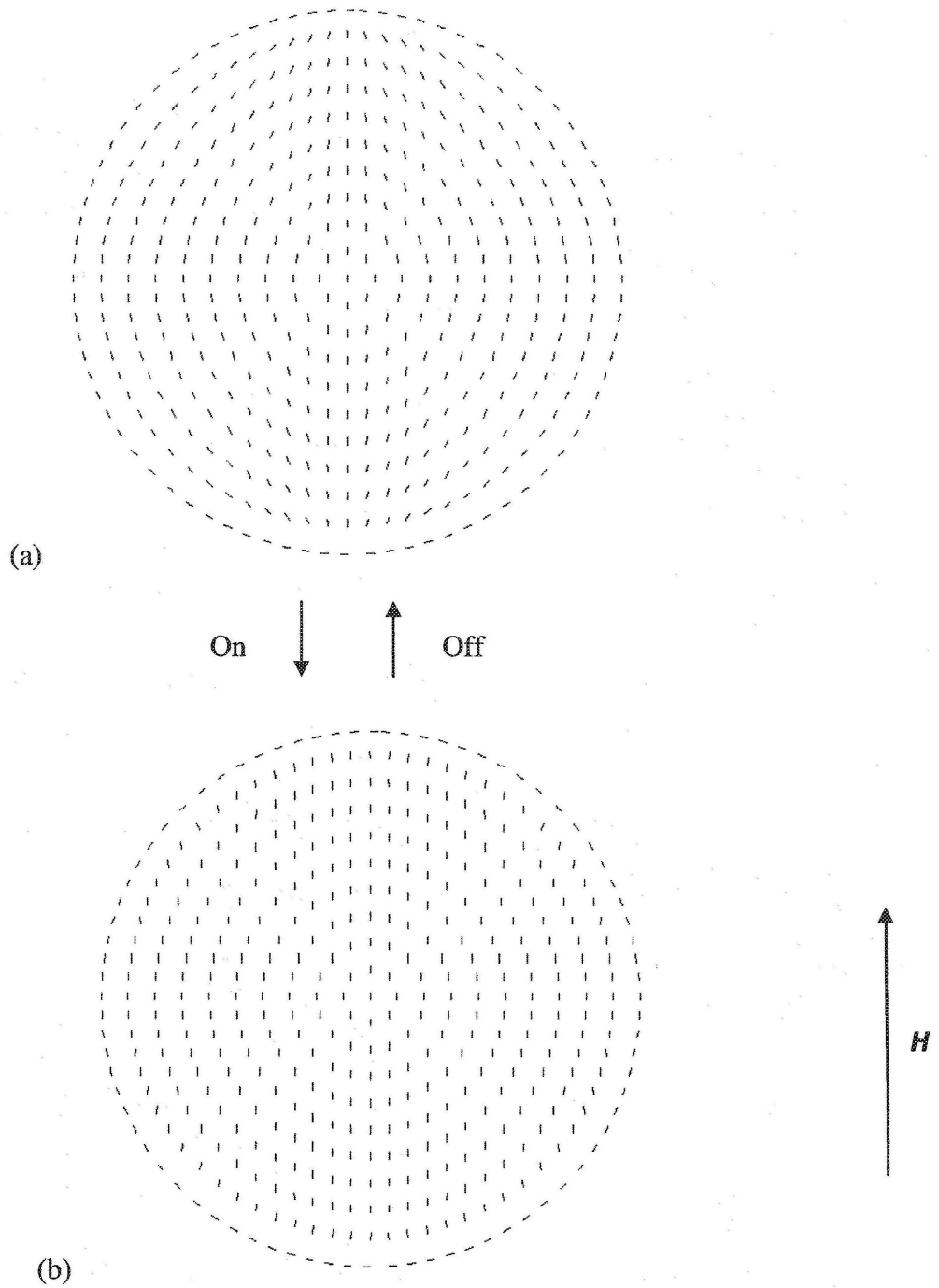


Figure 12. Simulation with FEM, $Z_o = 2000$, $c = 1$, $k_{11} = 0.6667$ and $k_{33} = 1.3333$. (a) Initial condition and (b) steady state condition with external field applied parallel to the droplet.

4.1.2 Simulation with Finite Difference method

In this section, result of simulation of a bipolar droplet with FDM is presented. Steps described in section 3.1.2.1 were taken.

Figure 13 shows the initial condition (a), and steady state condition, (b) when external field is turned on. In the beginning, (a), the droplet is in its bipolar configuration. Upon application of magnetic field the molecules align with the external field. Z_o , c , k_{11} , and k_{33} have the same value as in Figure 12. It is observed that in both cases (Figure 12 and Figure 13) after applying the external field, the molecules reorient and align with the field.

Besides, mesh refinement is carried out to find the optimum number of elements necessary for the simulation. The criterion is when the change in steady state mean magnitude of orientation angle $\langle |\phi_{st.on}| \rangle$ is less than 0.001 during the time when external field is on. Results of mesh refinement indicate optimum number of element to be 221. In system analysis and optimization section 221 elements is used for simulation of a single droplet.

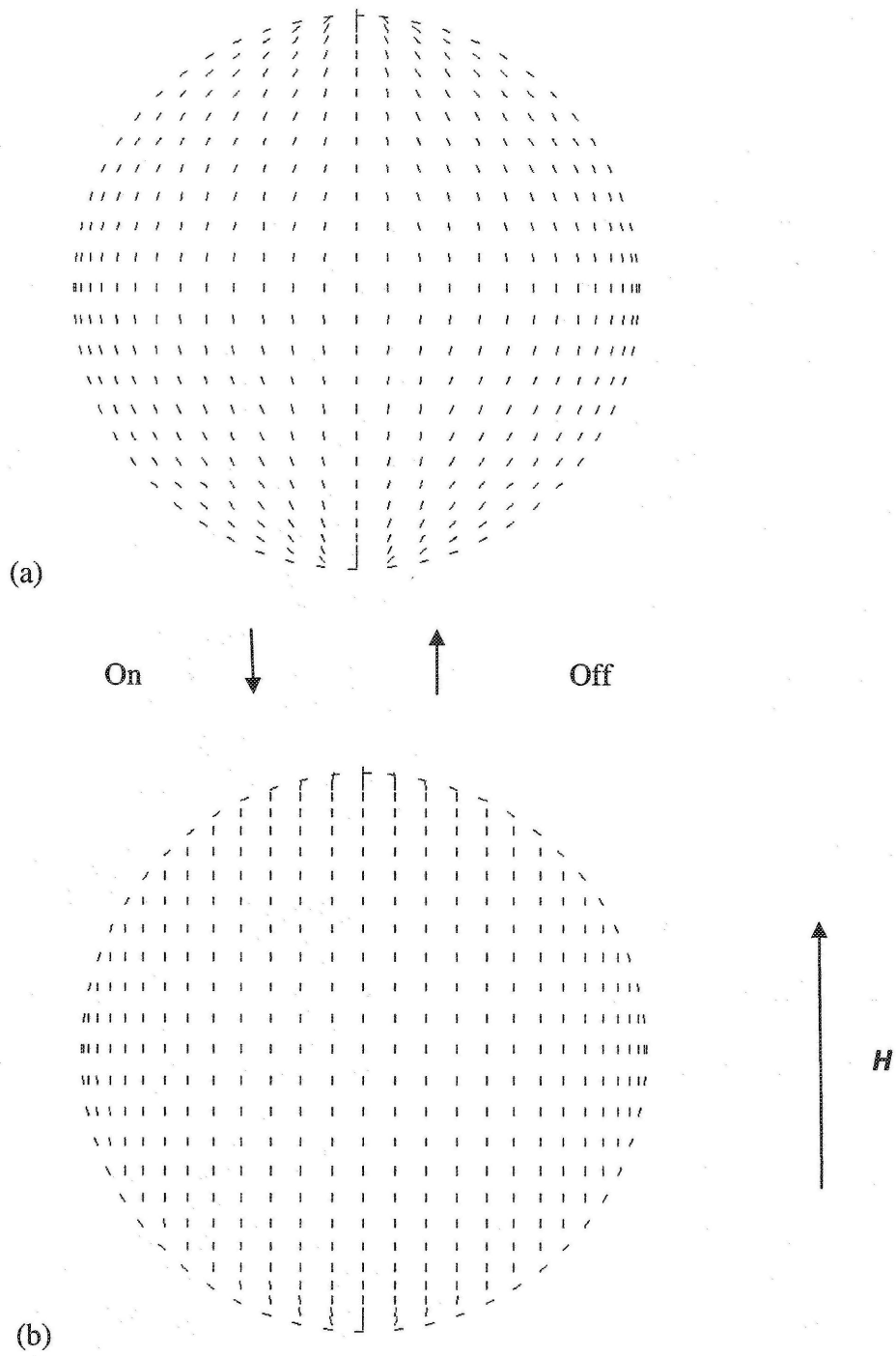


Figure 13. Simulation with FDM, $Z_0 = 2000$. $c = 1$, $k_{11} = 0.6667$ and $k_{33} = 1.3333$. (a) Initial condition and (b) steady state condition with external field applied parallel to the droplet.

4.1.3 Comparison of FDM and FEM simulation results

The results of FDM simulation are compared with FEM results to verify the applicability of two methods. In order to do so, numerical values of orientation angle in each grid point should be compared with FEM numerical results. In section 4.1.3, FEM is run with FDM mesh and mean magnitude of orientation angle is compared in each time step.

All variables have the same value ($c = 1$, $Z_o = 2000$, $k_{33}/k_{11} = 2$). Mesh presented in Figure 9 is used as initial condition. Figure 14 shows the steady state condition with external field applied parallel to the droplet axis of symmetry. The left half of circle represents the FEM results and the right half represents the FDM results. It is observed that in both simulations the molecules are reoriented and aligned with the magnetic field, the results of reorientation are identical in two half circles.

The behavior of $\langle |\phi| \rangle$ over time is compared in FDM and FEM. Behavior of $\langle |\phi| \rangle$ over time in FDM is presented in Figure 15, and behavior of $\langle |\phi| \rangle$ over time in FEM is presented in Figure 16. The mean magnitude of orientation angle is defined according to Equation 31.

In Figures 15 and 16 the field is on during dimensionless time 0-0.1, and after that external field is turned off and director goes back to its initial condition. The behavior of $\langle |\phi| \rangle$ over time is identical in two figures. It can be seen in Figure 15 that response time, the time required for director to reach the steady state condition with magnetic field > 0 is smaller than relaxation time, time required for director to reach steady state condition when external field is turned off. Response time and relaxation time are further studied in section 4.2.

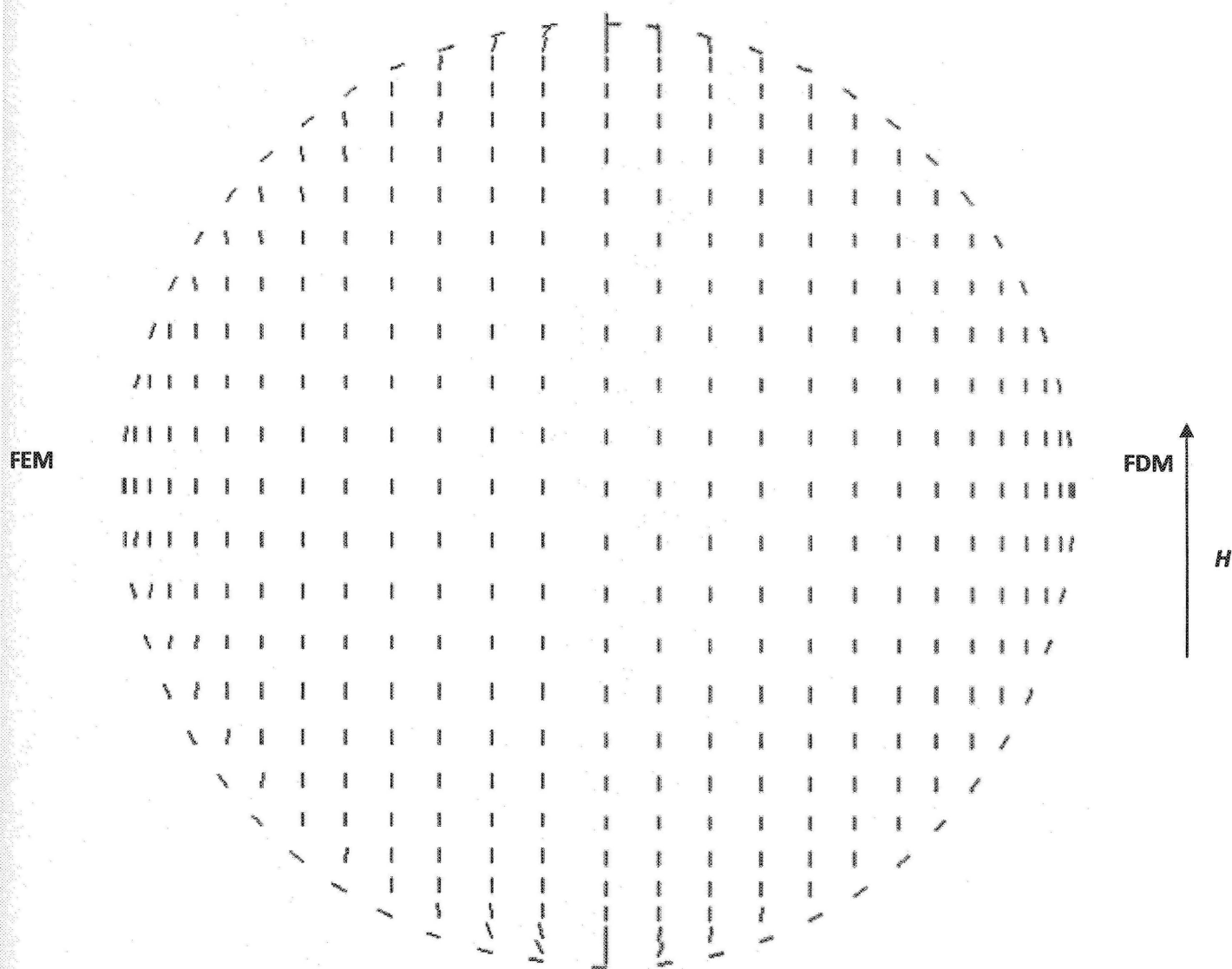


Figure 14. Steady state conditions with external field applied parallel to the droplet axis of symmetry. $Z_0 = 2000$, $c = 1$. Left half of the circle represents the FEM simulation results, and right half of circle presents the FDM simulation results.

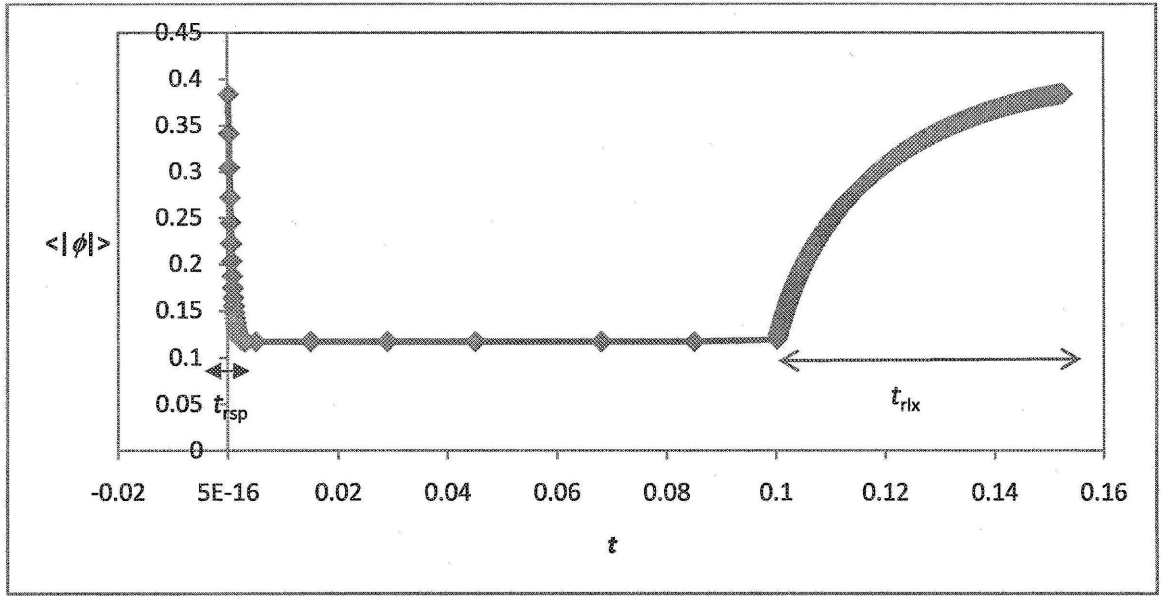


Figure 15. Mean magnitude of orientation angle versus time in FDM simulation, for $c = 1$, $Z_o = 2000$, $k_{33}/k_{11} = 2$. External field is on during 0-0.1, and is off during 0.1-0.16. t_{rsp} and t_{rlx} are presented.

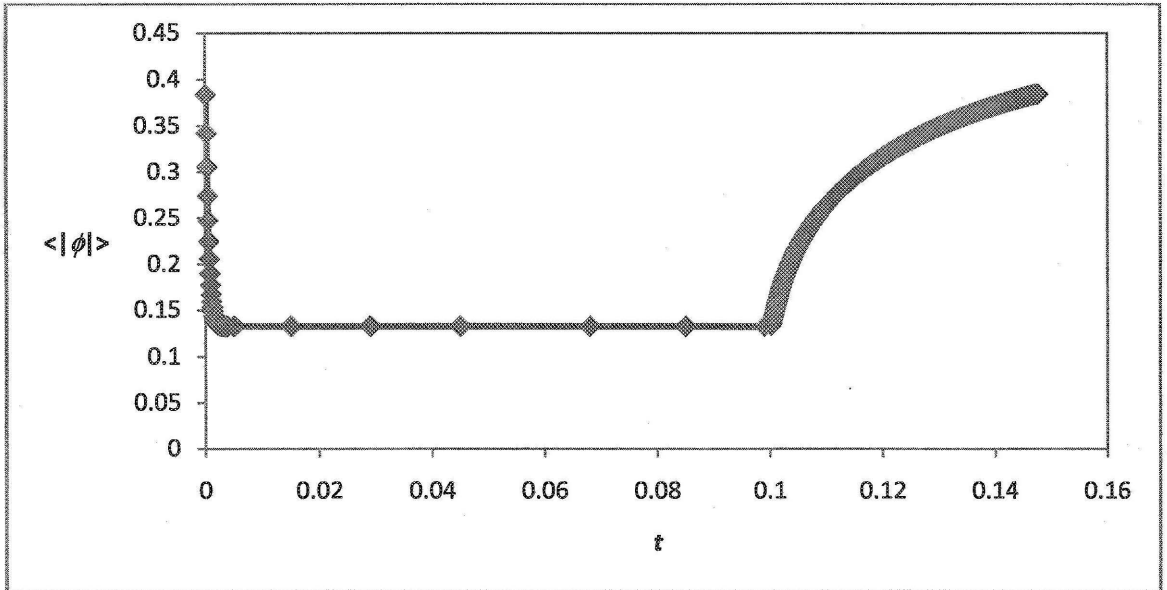


Figure 16. Mean magnitude of orientation angle versus time in FEM simulation, for $c = 1$, $Z_o = 2000$, $k_{33}/k_{11} = 2$. External field is on during 0-0.1, and is off during 0.1-0.16.

In Figures 15 and 16, when external field is turned on, the average orientation angle $\langle|\phi\rangle$ reduces sharply and then remains constant with time. During this time the molecules align with the external field. After $t = 0.1$ field is turned off and molecules go back to their initial condition; as a result $\langle|\phi\rangle$ goes back to its initial value. Results of numerical values for $\langle|\phi\rangle$ in FDM and FEM simulations are presented in Table 1.

Table 1 Comparison of numerical values of $\langle|\phi\rangle$ in simulations with FDM and FEM.

Dimensionless Time		$\langle \phi\rangle$ in FDM	$\langle \phi\rangle$ in FEM
0	(initial condition)	0.38494	0.38494
0.01	(steady state On)	0.12042	0.12981
0.1	(initial condition Off)	0.12042	0.12981
0.15	(steady state Off)	0.38480	0.38480

It is observed that the values of $\langle|\phi\rangle$ follow are similar in both simulations. There is slight difference (10^{-3}) in numerical value of $\langle|\phi\rangle$ in steady state condition with external field on. The reason is difference in methods of simulation. In both simulations mean magnitude of orientation angle follow the same trend, and the FDM is verified.

The CPU time for simulation of a single nematic droplet with specific aspect ratio ($c = 1$), elastic constant ratio ($k_{33}/k_{11}=2.0$), and external field strength ($Z_0= 2000$) was measured for a 2 GHz laptop. FDM gives the answer in 5 seconds where FEM gives results in 30 seconds. System analysis and optimization are based on FDM program, because it is six times faster method in comparison to FEM in simulation of a nematic droplet. Since there is no analytical solution present for modeling the behavior of a single droplet in a magnetic field, the accuracy of the results with two methods cannot be compared adequately. However, mean magnitude of orientation angle is similar in both simulations and follow the same pattern.

4.2. System analysis

The effect of physical properties, shape of droplet, and external field strength is studied on performance of PDLC films in section 4.2.1- 4.2.5. The performance criteria are response time and relaxation time.

4.2.1. Effect of aspect ratio on response time and relaxation time

Aspect ratio is changed from 1 to 2, as droplet goes from spherical to an elongated shape. The effect of this change on response time and relaxation time is studied.

Figure 17 shows the change in response time with aspect ratio for spherical droplet ($c = 1$) $Z_0 = 3000$ and $k_{33}/k_{11} = 2$. It is observed that response time increases by the aspect ratio of the droplet. Drzaic [3] has observed this phenomena and he explained that molecules in a spherical droplet

are more curved than molecules inside an elongated droplet. The response time is a function of distortion energy of molecules inside the droplet, and highly curved molecule have more distorted energy and responses to the external field faster than a less curved molecule. As a result response time increases by aspect ratio.

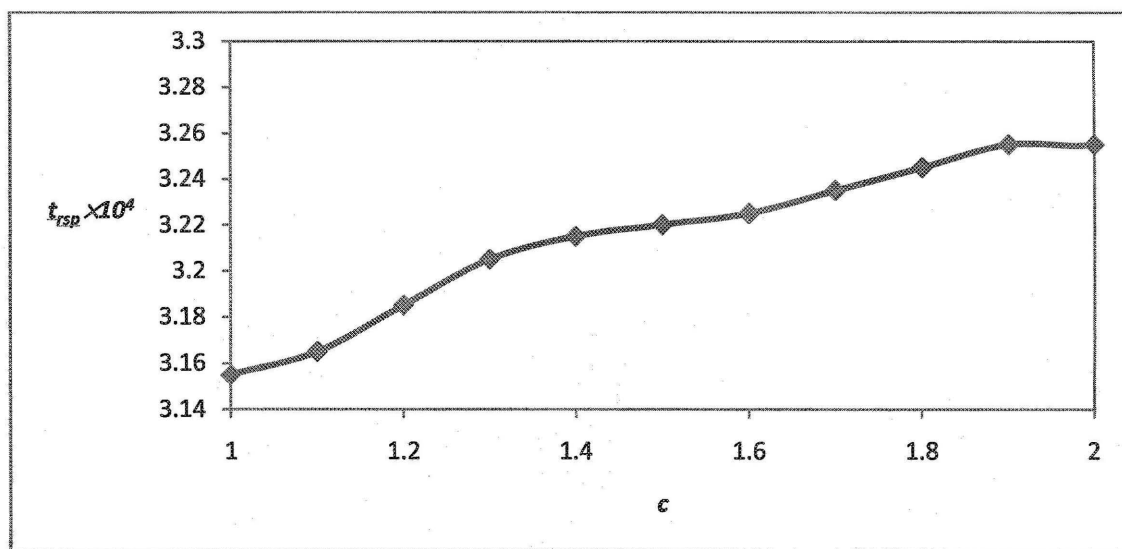


Figure 17. Response time versus aspect ratio, $Z_0=3000$ and $k_{33}/k_{11}=2$.

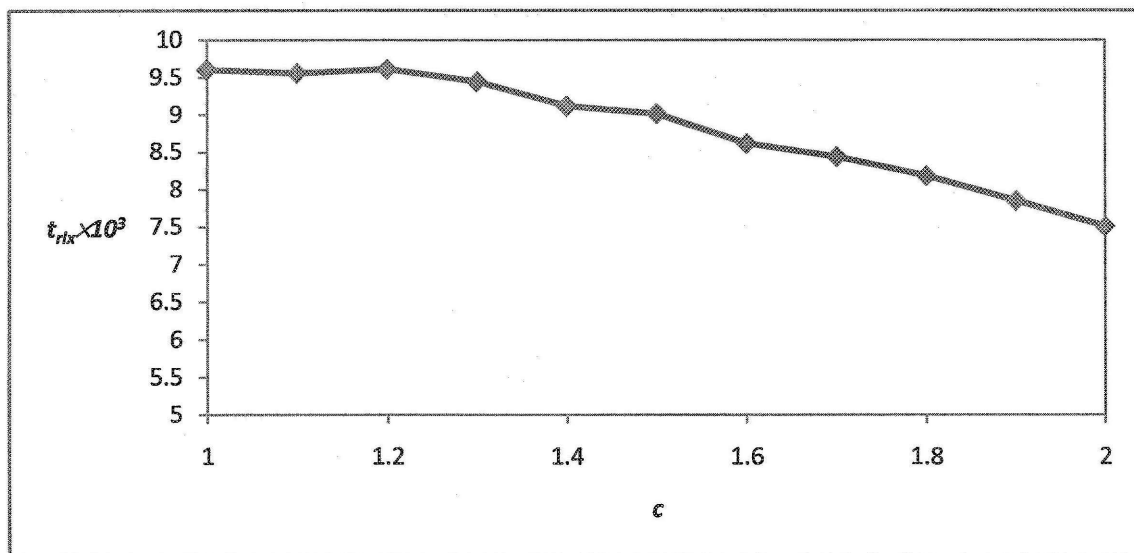


Figure 18. Relaxation time versus aspect ratio for $Z_o = 3000$ and $k_{33}/k_{11} = 2$.

Figure 18 shows the effect of aspect ratio on relaxation time. It is observed that relaxation time decreases as the aspect ratio increases. Because the droplet with higher aspect ratio is distorted less than a spherical droplet when it reaches $\langle |\phi_{st.on}| \rangle$, as a result upon removal of external field it reaches the initial condition faster than spherical droplet [10].

Besides, Figures 17 and 18 show that response time is one order of magnitude smaller than relaxation time and the rate of change in response time is about one hundred time smaller than rate of change in relaxation time.

4.2.2 Effect of external field strength on response time and relaxation time

Strong external field means high energy and an expensive device. Figure 19 represents the response time versus magnetic field strength. This figure shows that response time decreases with external field strength because of increase in H which reduces t .

Effect of magnetic field strength on relaxation time was also studied. Results show that relaxation time is not a function of field strength. In off state $\Gamma_m = 0$.

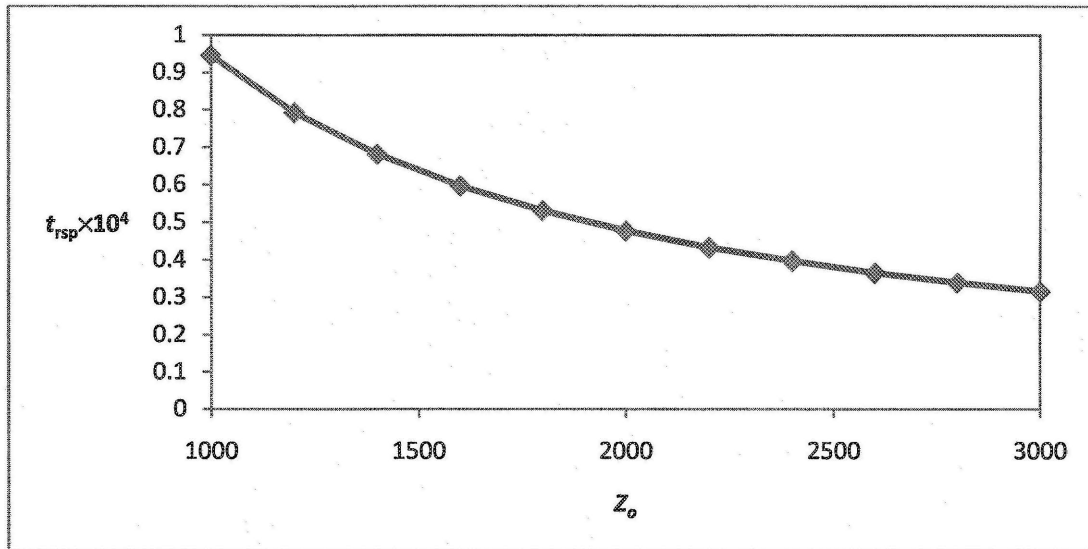


Figure 19. Response time versus Z_0 for $c = 1.5$, $k_{33}/k_{11} = 2$.

4.2.3 Effect of elastic constant ratio on response time and relaxation time

In this work, effect of splay and bend elastic constant is studied on performance of PDLC films. As simulation is restricted to a nematic droplet in two dimensions there is no twist deformation presented.

In a nematic droplet k_{33}/k_{11} is in range of 1-16 [33]. Above this range nematic droplet change to smectic with more positional order in molecules. Bipolar configuration is achieved for droplet with k_{33}/k_{11} between 1.1 and 2.3 [36]. Effect of elastic constant ratio on response time is measured to be less than 10^{-6} for Z_o between 1000 and 3000. This change is very small because of strong external field strength which dominates magnetic torque in Equation 1. But effect of elastic constant ratio is significant on relaxation time (Figure 20). As expected relaxation time increases with elastic constant ratio, because of more positional order inside the droplet with high elastic constant ratio, the molecules resist more to change in orientation than a molecule with less positional order.

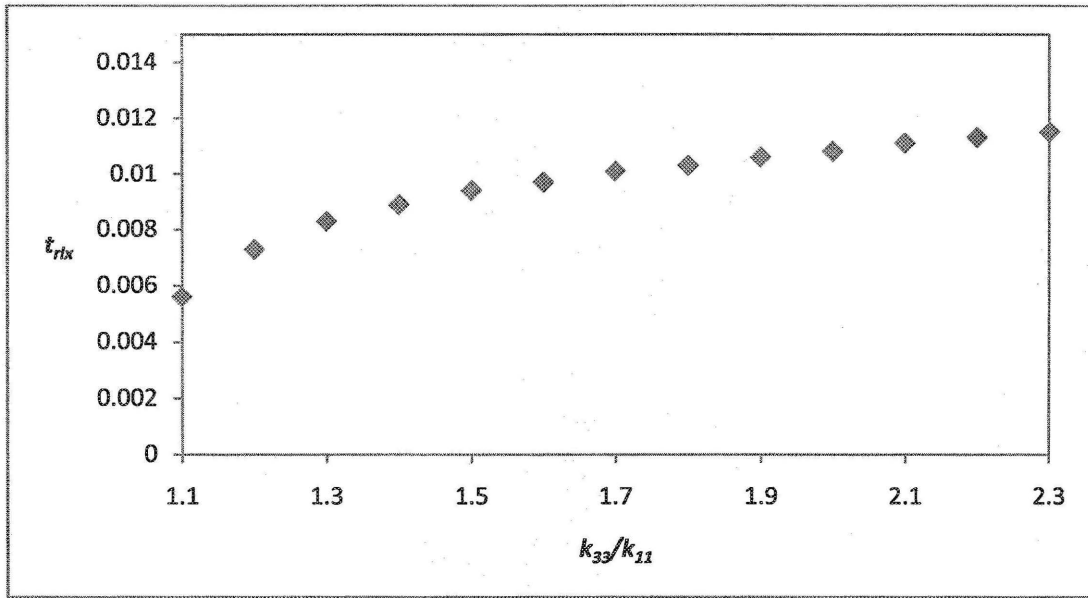


Figure 20. Relaxation time versus k_{33}/k_{11} . $Z_o = 3000$, and $c = 1$.

4.2.4 Effect of aspect ratio and external field strength on sum of response and relaxation time

In this section, elastic constant ratio is fixed ($k_{33}/k_{11} = 2$) and effect of the two other variables, aspect ratio of droplet and external field strength, on sum of response time and relaxation time is studied. The goal is to have minimum relaxation and response time. An objective function which is summation of relaxation time and response time is defined as:

$$J_{M1} = J_1 + J_2 = \frac{t_{rsp} - t_{rsp(min)}}{t_{rsp(max)} - t_{rsp(min)}} + \frac{t_{rlx} - t_{rlx(min)}}{t_{rlx(max)} - t_{rlx(min)}} \quad (40)$$

According to sections 4.2.1-4.2.3 maximum response time ($t_{rsp(max)}$) is achieved at $Z_o = 1000$ and $c = 2$. Minimum response time ($t_{rsp(min)}$) is achieved at $Z_o = 3000$ and $c = 1$. Maximum relaxation time ($t_{rlx(max)}$) is achieved at $c = 1$ and $k_{33}/k_{11} = 2.3$, and minimum relaxation time ($t_{rlx(min)}$) is achieved for a droplet with $c = 2$ and $k_{33}/k_{11} = 1.1$.

The results of simulation are shown in Figure 21. The vertical axis represents the objective function. Each curve represents a specific Z_o , and the aspect ratio in each curve changes from 1 to 2, Z_o has a major effect on reduction of response time (Figure 19) and as a result Objective Function value decreases by Z_o .

In each curve elongated droplet ($c = 2$.) results in minimum objective function. The higher the external field strength, the less is objective function value. However, higher external field strength results in more energy consumption. And one of the objectives of this work is finding the minimum field strength that reorients the molecules inside the droplet. Besides, in this figure it is not possible to study the effect of elastic constant ratio on objective function. Minimization of energy and effect of elastic constant ratio of molecules in droplet are studied in optimization section (4.3).

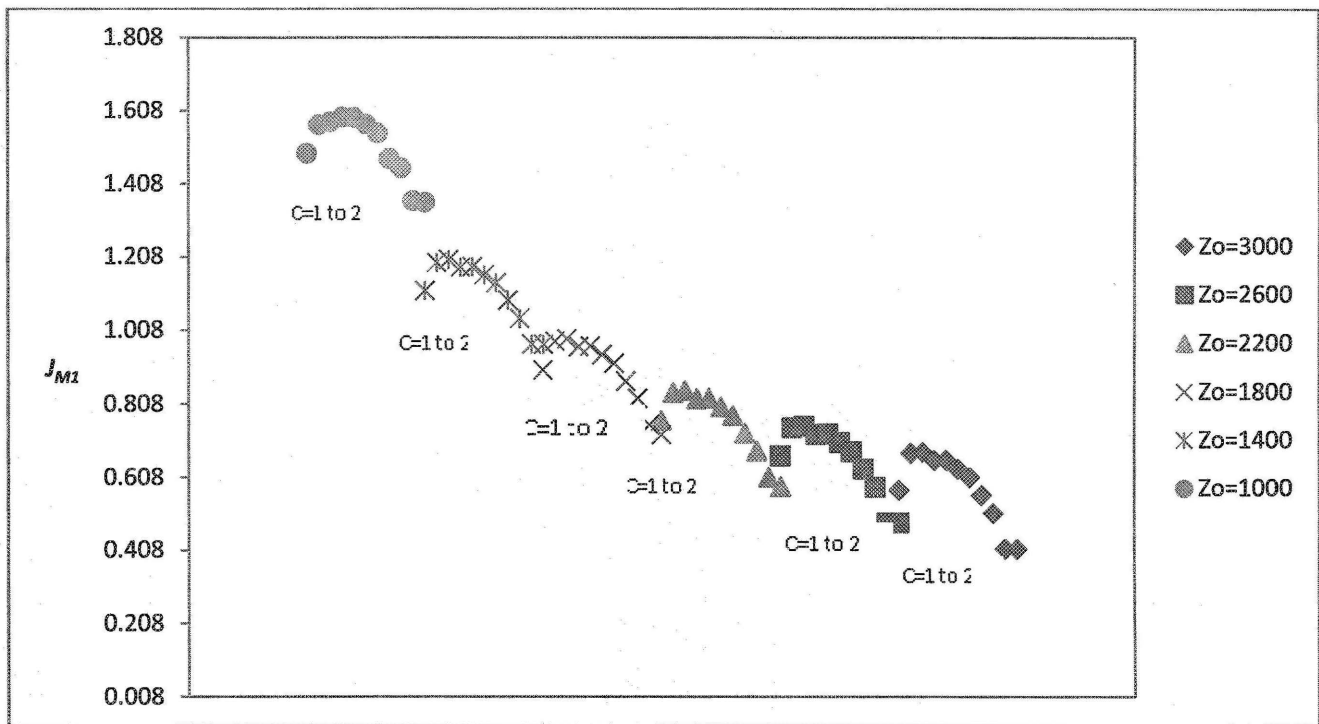


Figure 21. J_{MI} (Equation 40) for different Z_o . Each curve represents a specific Z_o , the aspect ratio in each curve changes from 1 to 2. $k_{33}/k_{11} = 2$.

4.2.5 Effect of aspect ratio and elastic constant ratio on sum of response time and relaxation time

By fixing the value of Z_o , it is possible to study the effect of elastic constant ratio and aspect ratio on response time and relaxation time. In this section, elastic constant ratio is changed in range of 1.1 to 2.3 [36]. Aspect ratio of droplet is changed from 1 to 2. Effect of these two variables is studied on J_{MI} (Equation 40). $Z_o = 3000$. Figure 22 shows that elongated droplet are optimal for they result in minimum J_{MI} value. By increasing elastic constant ratio the objective function

(J_{MI}) value increases, because of more positional order in droplet with high elastic constant ratio [33].

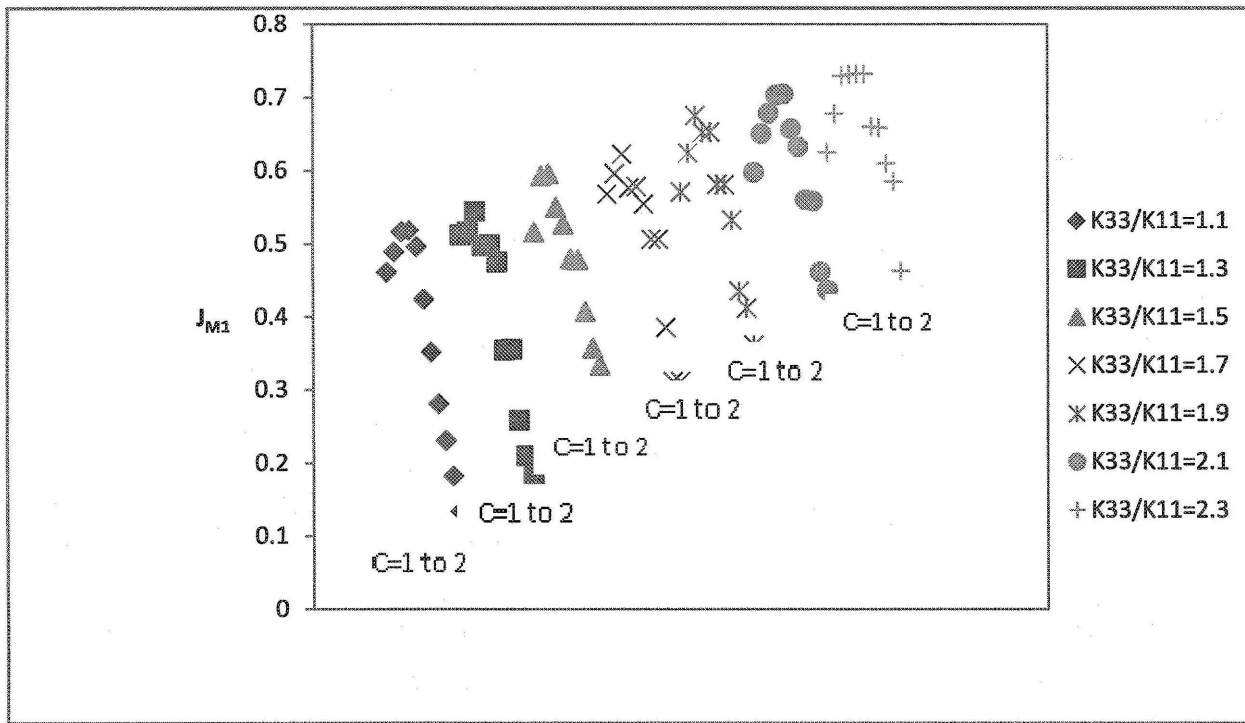


Figure 22. J_{MI} (Equation 40) for different elastic constant ratios. Each curve represents a specific bend to splay constant ratio, the aspect ratio in each curve changes from 1 to 2. $Z_o = 3000$.

4.3 Optimization

Multi-Objective Genetic Algorithm is employed to find the optimum aspect ratio of droplet, elastic constant ratio of molecules inside the droplet, and external field strength applied to PDLC films. Results of optimization are presented in this section.

GA is one of the nontraditional optimization methods. It can handle complex optimization problems, and is famous for being a robust, global searcher. As a result GA is used in optimization part of this research work.

First, optimization program is tested with number of testing functions for unconstrained optimization. The behavior of these test problems varies to cover most difficulties faced in the area of continuous global optimization. Result of optimization with three different test functions (Booth, Beale, and Easom functions) are presented in Appendix C. Sections 4.3.1-4.3.2 describe the result of optimization on PDLC films performance.

4.3.1. Optimization of PDLC films performance

The optimization problem consists of objective function, variables and their limits:

$$J_{M2} = J_1 + J_2 + J_3 = \frac{t_{rsp} - t_{rsp(min)}}{t_{rsp(max)} - t_{rsp(min)}} + \frac{t_{rlx} - t_{rlx(min)}}{t_{rlx(max)} - t_{rlx(min)}} + \frac{Z_o - Z_{o(min)}}{Z_{o(max)} - Z_{o(min)}} \quad (41)$$

Variables and their limits;

Aspect ratio of droplet c $1.0 < c < 2.0$

Elastic constant ratio k_{33}/k_{11} $1.1 < \frac{k_{33}}{k_{11}} < 2.3$

External field strength Z_o $1000 < Z_o < 3000$

For solving this optimization problem the random number generator uses the time function to generate the seed number; as a result seed number is randomly generated. Effect of loop number and population size is studied on optimization results. Loop number is changed from 50 to 1000, and population size is changed from 50 to 750. Effect of population size and loop number on optimization results are presented in Table 2 and 3.

Table 2. Optimization results (effect of population size). Loop number is fixed on 200.

Population size	c	k_{33}/k_{11}	Z_o
50	1.17	1.99	1903
100	1.14	1.978	1640
200	1.13	1.98	1660
300	1.13	1.98	1663
400	1.11	1.98	1660

500	1.11	1.98	1660
750	1.11	1.98	1660

It is observed that increasing the population size and loop number increases the accuracy in results. However, large population size and loops means longer computation time. In order to define the loop number and population size, the following error (Equation 42) is calculated. i presents the iteration number. Sensitivity analysis show that loop number of 200 and population size of 500 results in error less than 10^{-3} . As a result these values are used for optimization.

$$\frac{J_{M2}(i) - J_{M2}(i-1)}{I_i - I_{(i-1)}} < 10^{-3} \quad (42)$$

Multi-objective genetic algorithm with 500 populations and 200 loops is run for 20 times. Each variable is coded in genes of 15 bits. One run of GA with parameters stated in Table 4 takes 24 hours on a dual core 2. GHz laptop.

Table 3. Optimization results (effect of loop number).population size is fixed on 500.

Loop number	c	k_{33}/k_{11}	Z_o
50	1.1046	1.99	1603
100	1.112	1.97	1640

150	1.103	1.98	1660
200	1.100	1.99	1690
500	1.11	1.99	1680
1000	1.11	1.98	1660

Parameters for GA are shown in Table 4.

Table 4. GA parameters for solving optimization problem in PDLC films performance.

Genetic algorithm	
Population	500
Loops	200
Gene size	15 bits
No. variables	3
Cross over rate	80%

Mutation rate	5%
Fitness function	$1/(1 + J_{M2})$
Seed number generator	Time of computer
No. Iteration	20

The fitness function is calculated based on FDM simulations. The criterion for optimum results is minimum fitness function value. In Table 5 the best results achieved in 20 times running the optimization program is presented. The optimum aspect ratio is achieved in range of $c \cong 2$. best elastic constant ratio is $\frac{k_{33}}{k_{11}} \cong 1.1$. Because of the sharp increase in relaxation time by elastic constant ratio (Figure 20) it is expected that small elastic constant ratio results in minimum objective function. Optimum value of external field strength is $Z_o \cong 1660$. This field strength is large enough to reorient the molecules completely upon application of external field, and at the same time minimum energy is applied to reorient molecules inside the droplet (Equation 41). The simulation results show that the elongated droplet are optimal because of their smaller relaxation time (Figure 18). The response time for an elongated droplet is more than spherical ones (Figure 17). However, response time is about one order of magnitude smaller than the relaxation time; as a result, the elongated droplet are recommended to be applied in PDLC devices.

Table 5. Optimization results (optimum results in 20 runs of GA).

Optimum c	Optimum k_{33}/k_{11}	Optimum Z_o	J_1	J_2	J_3
1.99	1.10	1660	0.4	0.05	0.33

Figures 23-25 show the results of optimization of 20 runs. Each figure shows the optimum value for each variable in 20 runs.

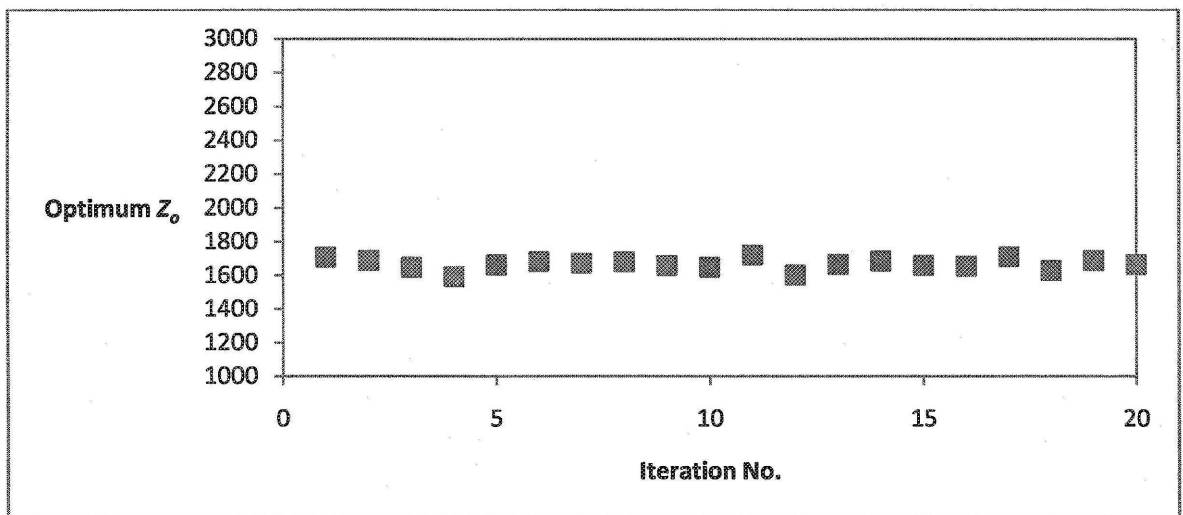


Figure 23. Optimum value of Z_o in 20 runs of optimization program.

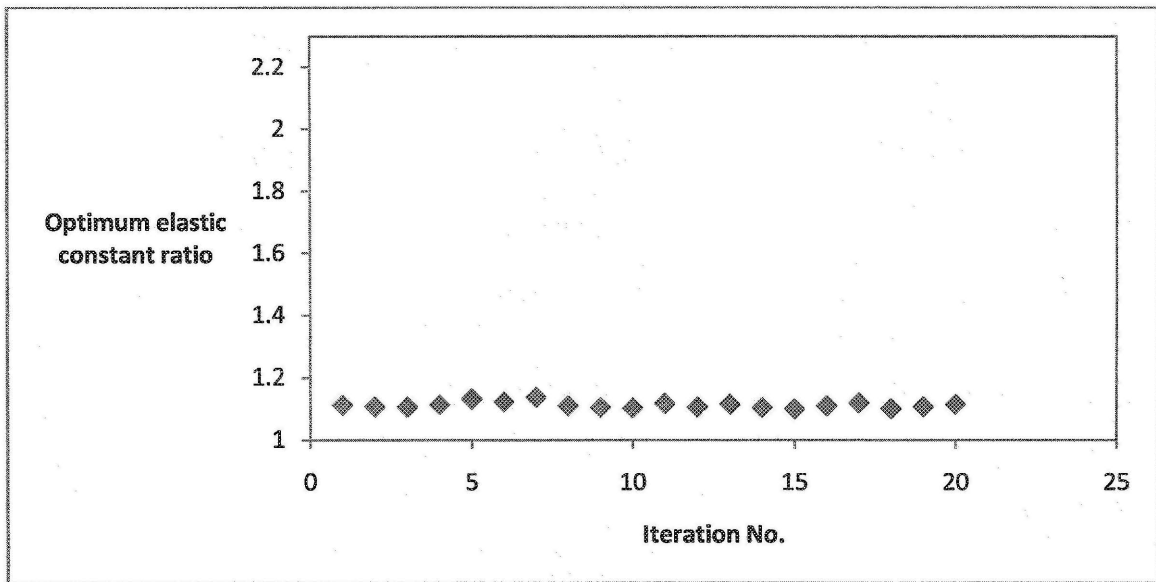


Figure 24. Optimum elastic constant ratios in 20 runs of optimization program.

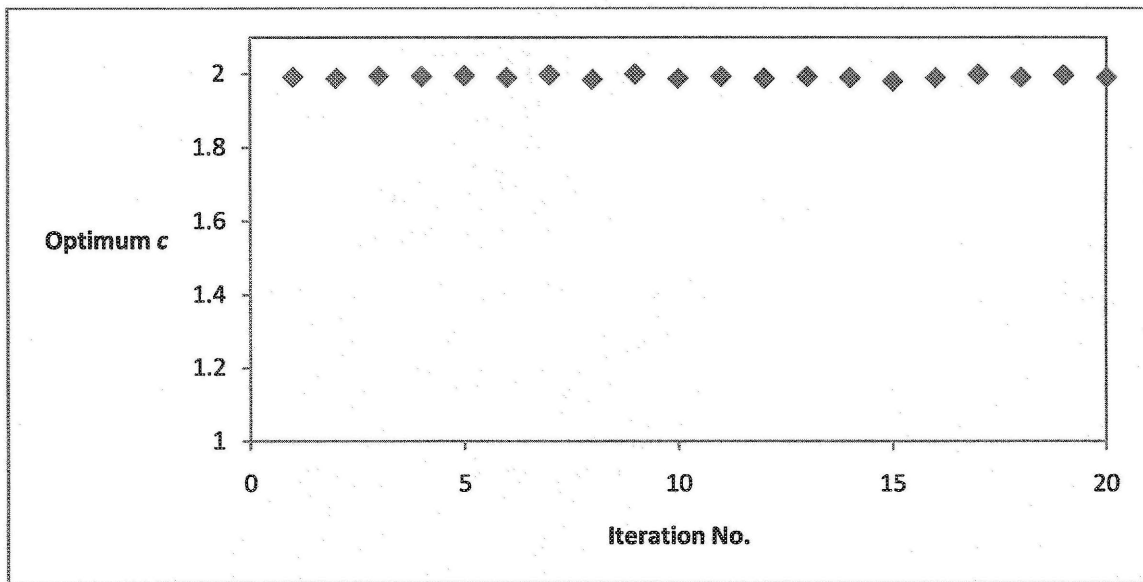


Figure 25. Optimum aspect ratios in 20 runs of optimization program.

4.3.2. Optimization of PDLC films performance (weighted objective functions)

In previous section (4.3.1), results of optimization of three objective functions with equal weights was presented. It is interesting to know the optimum aspect ratio, elastic constant ratio, and Z_0 with the weighted objective functions. In this section, J_1 , J_2 , and J_3 take different weights.

Results of weighted optimization are presented in Table 6.

Table 6. Optimization results for weighted J_{M2} ,

Weights of J_1, J_2, J_3	Optimum c	Optimum k_{33}/k_{11}	Optimum Z_0	J_{M2}	J_1	J_2	J_3
0.1 0.1 0.8	1.96	1.1	1000	0.1011	0.92	0.08	0
0.1 0.2 0.7	1.98	1.1	1000	0.1092	0.92	0.08	0
0.1 0.8 0.1	1.88	1.1	1678	0.1169	0.38	0.05	0.33
0.1 0.7 0.2	1.98	1.13	1300	0.1811	0.92	0.08	0.15
0.2 0.1 0.7	1.99	1.17	1000	0.1940	0.92	0.08	0
0.2 0.3 0.5	1.96	1.11	1036	0.2108	0.88	0.08	0.01
0.2 0.5 0.3	1.89	1.1	1400	0.1992	0.55	0.05	0.2
0.2 0.7 0.1	1.97	1.11	2600	0.1194	0.1	0.02	0.8
0.25 0.25 0.5	1.99	1.12	1300	0.2355	0.61	0.02	0.15

0.25	0.5	0.25	1.94	1.23	1700	0.2117	0.38	0.05	0.35
0.3	0.2	0.5	1.95	1.12	1400	0.2739	0.54	0.05	0.2
0.3	0.5	0.2	1.98	1.13	2400	0.1967	0.14	0.02	0.7
0.4	0.2	0.4	1.97	1.13	1600	0.2969	0.42	0.02	0.3
0.5	0.2	0.3	1.95	1.1	2500	0.2932	0.11	0.05	0.75
0.5	0.3	0.2	1.93	1.22	2700	0.2211	0.08	0.02	0.85
0.7	0.1	0.2	1.97	1.19	2980	0.2235	0.02	0.05	0.99
0.7	0.2	0.1	1.91	1.2	2996	0.1309	0.02	0.05	0.99
0.8	0.1	0.1	1.9	1.13	2990	0.1279	0.02	0.05	0.99

Results of optimization with weighted objective function show that small elastic constant ratio $\frac{k_{33}}{k_{11}} \approx (1.1 - 1.2)$, and elongated droplet ($c \approx 2$) provide an optimum performance for PDLC films. High Z_o (≈ 3000) provides an optimum condition for PDLC films when the response time has large weight and energy efficiency has small weight. Relaxation time is not a function of Z_o and as a result, weight of J_2 does not affect the optimum Z_o .

It is expected that in cases where J_1 (response time) has highest weights in comparison to J_2 (relaxation time), the optimum aspect ratio be achieved at spherical droplet, ($c \approx 1$). However, Table 6 shows that in ranges where weight of J_1 is eight times bigger than weights of J_2 , elongated droplet ($c \approx 2$) provide an optimum condition. The reason is that change in response

time is 10^{-2} of change in relaxation time, and elongated droplet provides minimum J_{M2} in this range of weights. By further studying effect of weight ratios of J_1 and J_2 in Table 7, it is observed that spherical droplet ($c \approx 1$) result in an optimum performance when the weight of response time is about 100 times bigger than weight of relaxation time.

Table 7. Analysis of J_1 and J_2 .

Weights of J_1, J_2, J_3	Optimum c	Optimum k_{33}/k_{11}	Optimum Z_o	J_{M2}	J_1	J_2	J_3
0.98 0.01 0.01	1.02	1.1	2990	0.01	0	0.44	0.995
0.9 0.1 0.0	1.84	1.22	2990	0.03	0.028	0.05	0.995
0.8 0.1 0.1	1.9	1.13	2990	0.12	0.028	0.05	0.995

Table 8 shows result of weighted optimization with two objective functions. One J_i ($i = 1, 2, 3$) takes weight of 0 where the two other have same weights.

Table 8. Optimization results with two objective functions

Weights of J_1, J_2, J_3	Optimum c	Optimum k_{33}/k_{11}	Optimum Z_o	J_{M2}	J_1	J_2	J_3
0. 0.5 0.5	1.91	1.20	1000	0.02	0.98	0.04	0.0
0.5 0. 0.5	1.0	1.20	1600	0.32	0.34	0.99	0.3
0.5 0.5 0.	1.99	1.12	2990	0.05	0.05	0.05	0.99

Table 8 shows that in cases where response time and energy efficiency (J_1 and J_3) compete with same weights, optimum Z_o is achieved in range of 1600, and because effect of relaxation time is zero, optimum aspect ratio is around 1. All optimization results show that elastic constant ratio of bipolar droplet should be around 1.

5. Conclusions

FDM is found to be a faster method in simulation of this droplet than FEM in simulation of a single nematic bipolar droplet. FDM was employed to model the behavior of a single nematic bipolar droplet when an external field is applied parallel to the droplet's axis of symmetry. Results of modeling with FEM and FDM were compared and the results are identical. System analysis was carried out and effect of shape, physical properties, and external field strength was elicited on performance of PDLC films. Performance criteria for PDLC films are short relaxation time, response time, and small external field strength. Simulation results show that:

- 1) Response time is estimated to be one order of magnitude smaller than relaxation time.
- 2) Liquid crystals with small elastic constant ratio would have smaller relaxation time.

Effect of elastic constant ratio on the response time is insignificant.

Multi-objective optimization with genetic algorithm was first tested on several challenging optimization problems, and then it was employed to find optimum aspect ratio, elastic constant ratio, and Z_0 in PDLC films. Numerical results show that:

- 3) Elongated droplet ($c \cong 2$) would result in minimum response time in on state, and relaxation time in off state. Spherical droplet would provide an optimum condition when minimization of relaxation time is not interested.
- 4) Droplet with small elastic constant ratio ($\frac{k_{33}}{k_{11}} \cong 1.1$) would provide minimum response time in on state, and relaxation time in off state.

5) The external field with $Z_o \approx 1600-1800$ is estimated to be optimum field strength when minimization of response time and minimization of energy have similar weights. In cases where one is more interested in minimization of response time, high Z_o (≈ 3000) would provide an optimum condition.

6. Recommendation

In this research work, a bipolar nematic droplet was modeled in two dimensions and effect of bend and splay elastic constants on performance of PDLC films was studied. Recently there is interest in use of chiral nematic droplet in PDLC films [8]. By modeling a chiral nematic droplet in three dimensions, the optimum elastic constants and aspect ratio of the droplet, and external field strength can be defined for the PDLC films. Three dimensional modeling would enable one to study the effect of twist deformation.

Appendix A. Lagrange interpolating polynomial [35]

The Lagrange interpolating polynomial is the polynomial $P_i(x)$ of degree $< (q-1)$ that passes through the n points $(x_{i_1}, y_{i_1} = \text{fun}(x_{i_1}))$, $(x_{i_2}, y_{i_2} = \text{fun}(x_{i_2}))$... $(x_{i_n}, y_{i_n} = \text{fun}(x_{i_n}))$, and is given by:

$$P_i(x) = \sum_{j=1}^n P_j(x) \quad (\text{A.1})$$

Where

$$P_j(x) = y_{i_j} \prod_{\substack{k=1 \\ k \neq j}}^n \frac{x_i - x_{i_k}}{x_{i_j} - x_{i_k}} \quad (\text{A.2})$$

This polynomial is used mostly for approximation of functions with unequal spaced data points.

Appendix B. Reproduction of previous simulations by FEM in literature

Reproduction of previous simulations by Chan et al. [11] is presented here. Figure B.1 and B.2 shows the droplet with aspect ratio of $c = 1.5$, where the external field is applied normal to the droplet axis of symmetry. The effect of external field strength on reorientation of molecules inside the droplet is presented.

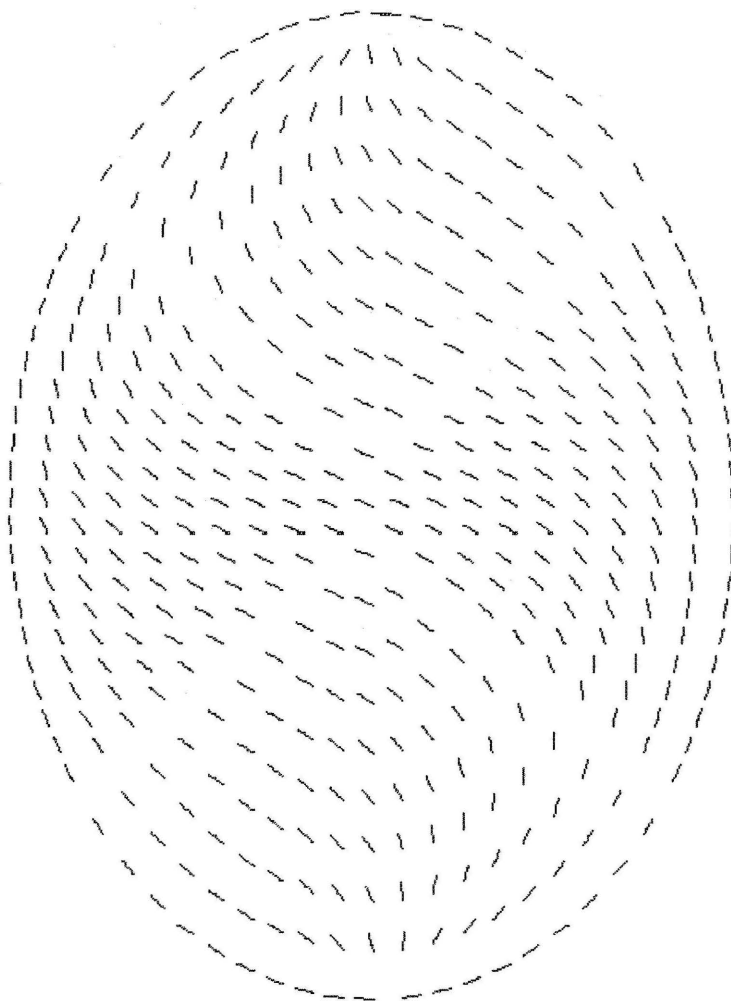


Figure B.1 Field applied normal to the droplet axis of symmetry. $Z_0 = 10$, $c = 1.5$

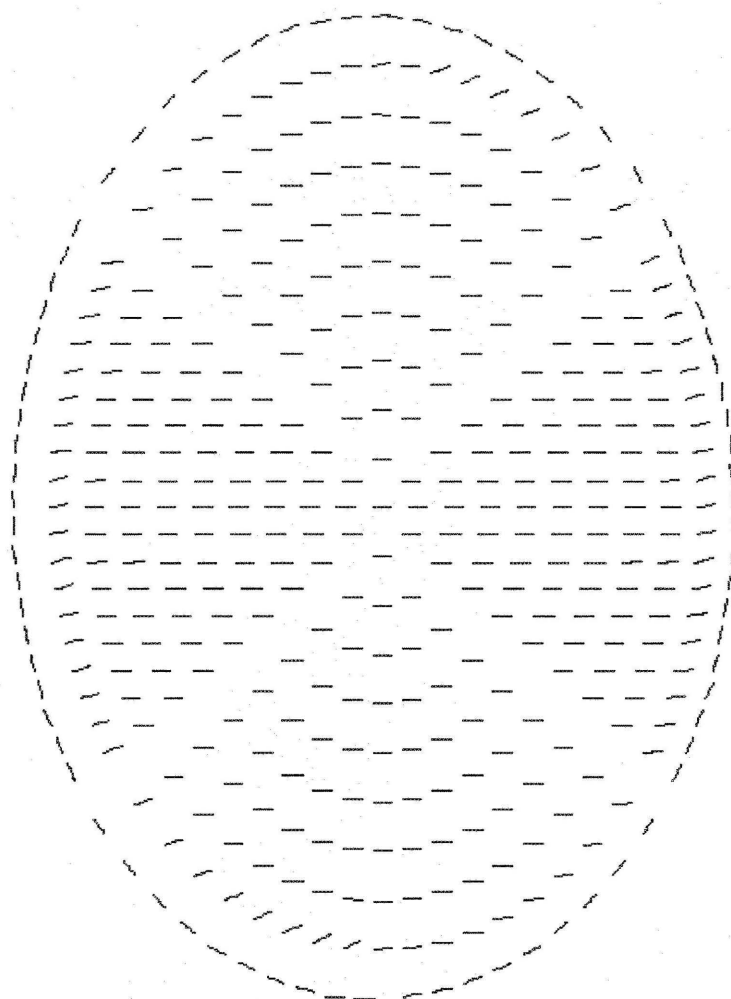


Figure B.2 Field applied normal to the droplet axis of symmetry. $Z_0 = 1000$, $c = 1.5$

Appendix C. Testing GA with test functions

GA is tested with a number of unconstrained global optimization test functions. Results are presented in this part.

Appendix C.1 Testing GA program with Booth function

Booth function is one of test functions for unconstrained global optimization. The specification for this function is presented in Table C.1. The function has several local minimums, with a challenging global optimum.

$$\text{Booth function} = (x_1 + 2x_2 - 7)^2 + (2x_1 + x_2 - 5)^2 \quad (\text{C.1})$$

Variables: x_1, x_2

Figure C.1 shows the three dimensional graph for booth function.

Table C.1 Booth function specifications

Booth function	
Number of variables	2
Search domain	$-10 \leq x_i \leq 10, i = 1,2$
Number of local minima	Several local minima

The global minimum

$$x^{min} = (1,3)$$

Objective function value in global minimum

$$f(x^{min}) = 0.$$

GA is tested on Booth function. Specifications of GA program are presented in Table C.2. The optimization problem is solved. Standard deviation of objective function is calculated to be $6.e-5$. The results of 80 runs of program with random seed numbers are presented in Fig.C.2. Results show the range for objective function value is 0-0.00034, where the function value at global minimum is 0.

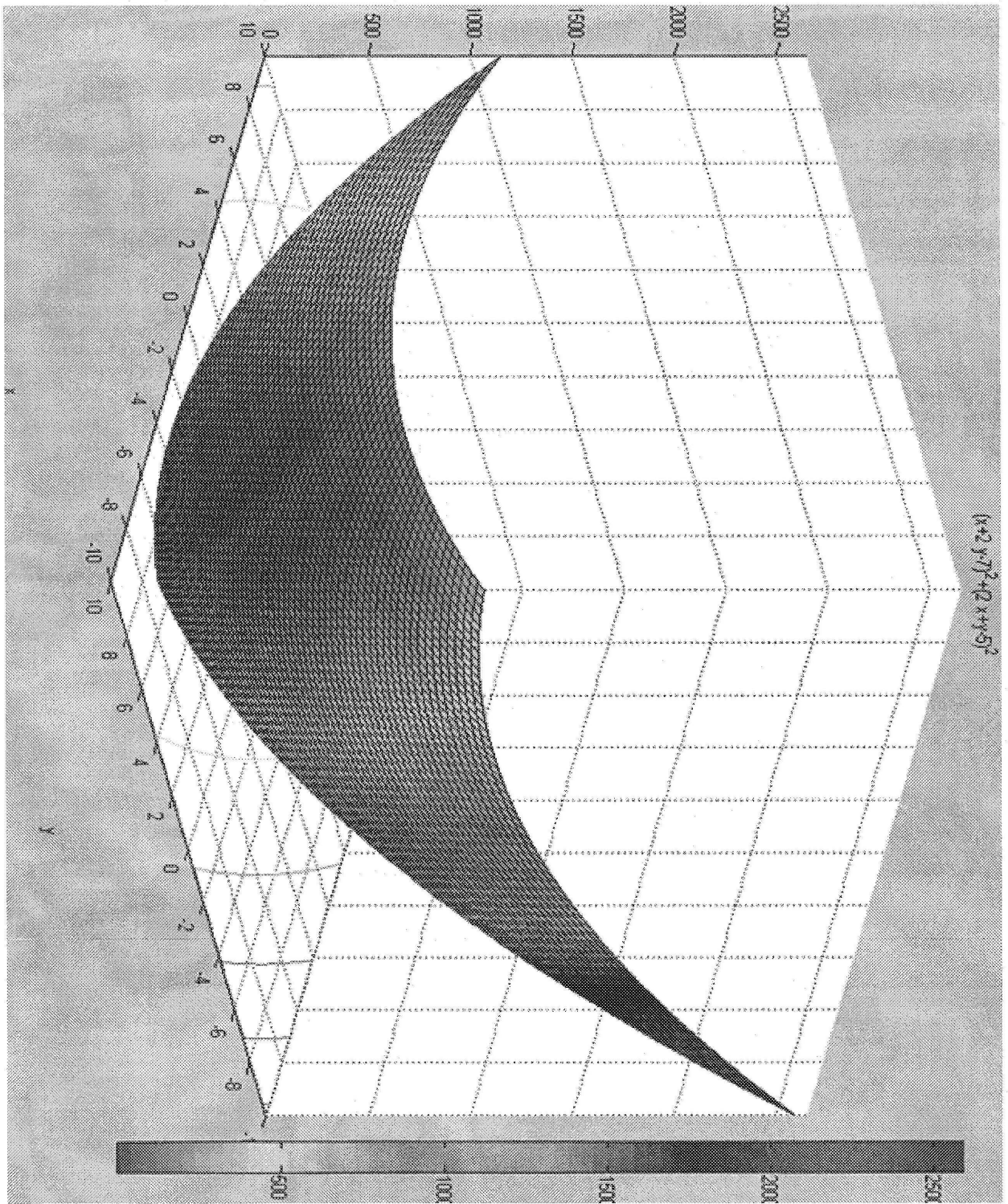


Figure C.1. Three dimensional graph for booth function, in the search domain range. Global minimum at (1, 3).

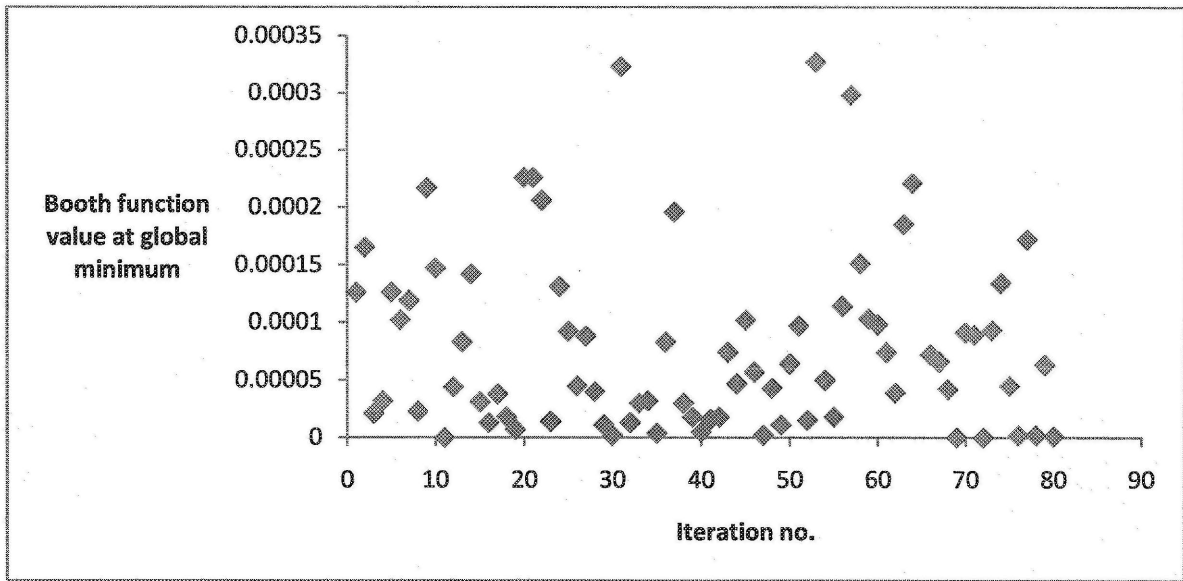


Figure C.2. Optimization results for 80 runs GA with random seed number. Results are in range 0.-0.00034. Standard deviation is 10^{-5} .

Table C.2. Genetic algorithm parameters for solving Booth function

Genetic algorithm	
Population	2000
Loops	1000
Gene size	15 bits
No. variables	2

Cross over rate	80%
Mutation rate	5%
Fitness function	$1/(1 + Booth\ function)$
Seed number generator	Time of computer
No. Iteration	80
Standard deviation	10^{-5}

Effect of loop number and population size is studied on optimization results. Loop number is changed from 100 to 2000, where the population size is fixed on 1000. Results are presented in Fig. C.3. It is observed that by increasing loop number, accuracy of results increase sharply and it saturates with loop number in the range of 600 loops. It is concluded that GA solves the booth optimization problem with accuracy of 10^{-4} in about 600 loops, and 1000 population size. The time for one run of program with the parameters presented in table 4 is 15 seconds.

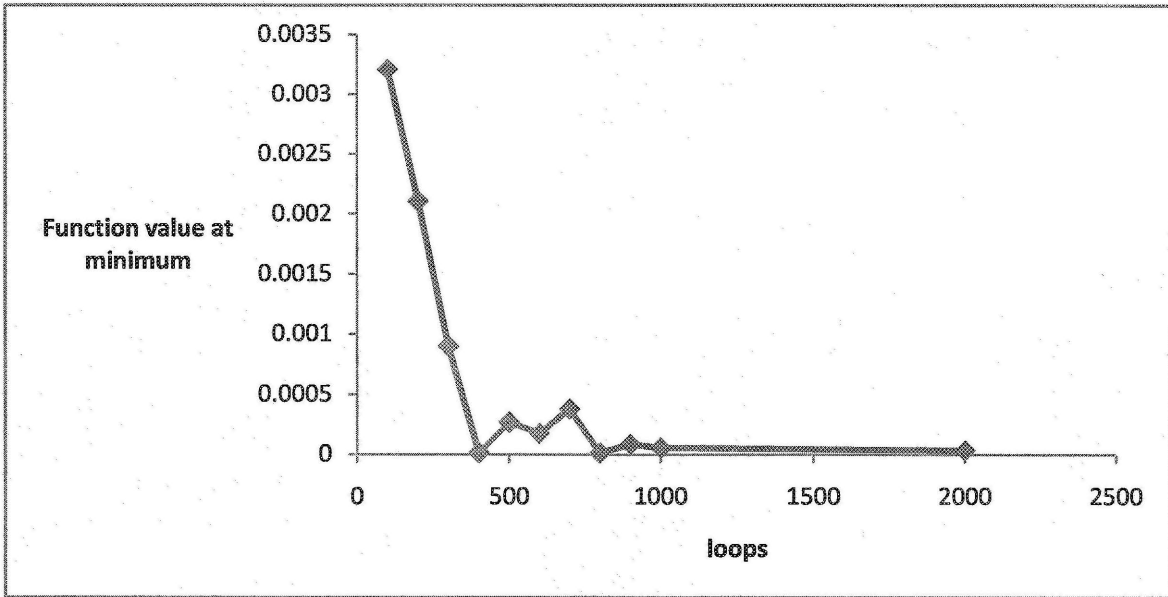


Figure C.3. Effect of loop number on optimum function value. By increasing the loop number, accuracy of optimization algorithm increases.

Effect of population size is studied on optimization results accuracy. In Fig. c.4 population size is changed from 100 to 2000, loop number is fixed on 1000. Results indicate that population size is an important factor in defining the optimization accuracy.

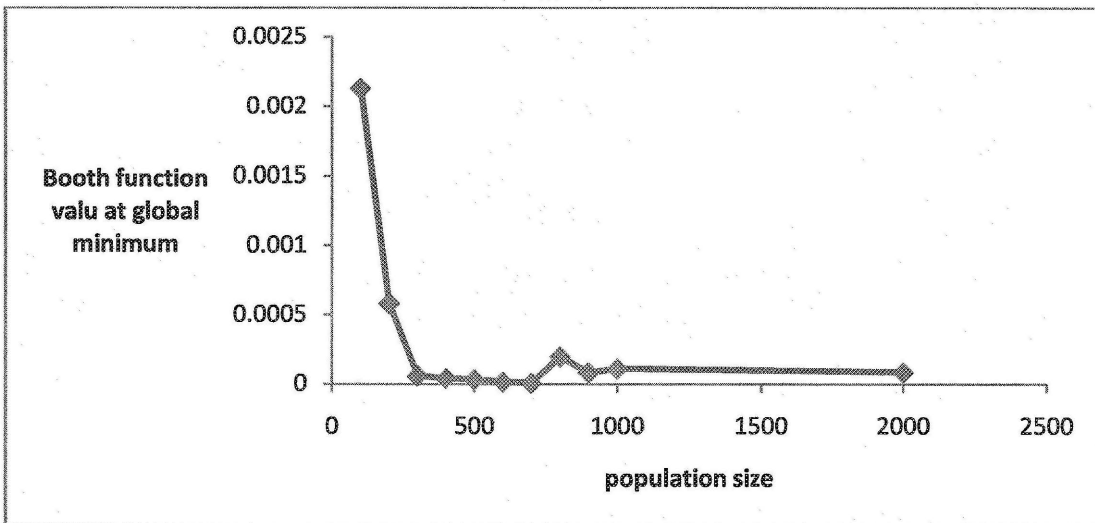


Figure C.4. Booth function value versus population size. Function value at global minimum is 0. By increasing population size, accuracy of results increases.

Appendix C. 2. Optimization of Beale function

Another test function for unconstrained optimization is Beale function and is expressed as:

$$\begin{aligned} \text{Beale function} = & (1.5 - x_1 + x_1x_2)^2 + (2.25 - x_1 + x_1x_2^2)^2 \\ & + (2.625 - x_1 + x_1x_2^3)^2 \end{aligned} \quad (\text{C.2})$$

Variables; x_1, x_2

This is a popular test function for global optimum searcher algorithms. Specifications of Beale function are presented in Table C.3. As you see Beale function has one global minimum at (3, 0.5), with several local minimums. Figure C.5 shows three dimensional graph of Beale function.

Table C.5 Beale function specifications

Beale function	
Number of variables	2
Search domain	$-4.5 \leq x_i \leq 4.5, i = 1,2$
Number of local minima	Several local minima
The global minimum	$x^{min} = (3,0.5)$
Objective function value in global minimum	$f(x^{min}) = 0.$

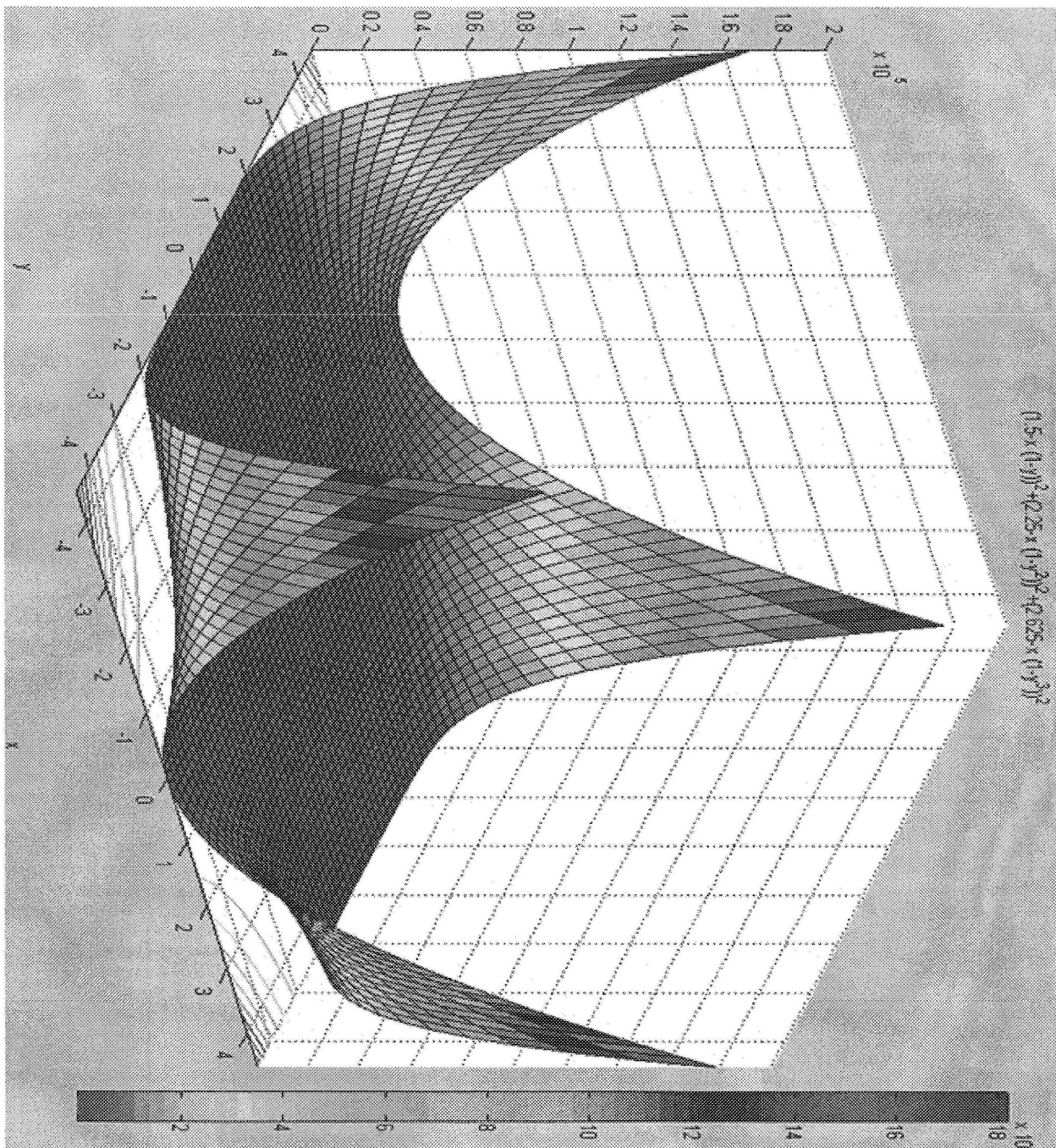


Figure C.5. Beale function.

Table C.4. GA specifications for solving Beale function

Genetic algorithm	
Population	2000
Loops	2000
Gene size	15 bits
No. variables	2
Cross over rate	80%
Mutation rate	5%
Fitness function	$1/(1 + \text{Beale function})$
Seed number generator	Time of computer
No. Iteration	90
% Standard deviation	10^{-3}

GA with specifications presented in table 6 is applied to solve Beale function. Program is run 90 times and standard deviation is calculated. Results of optimizations for 90 iterations are presented in Fig.C.6.

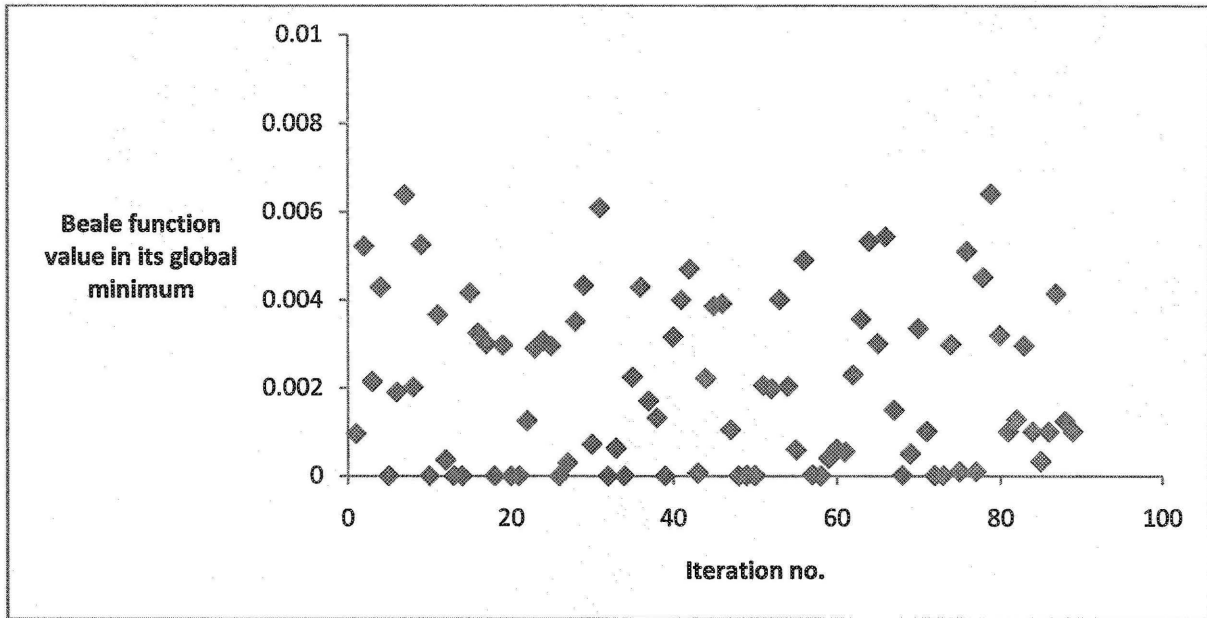


Figure C.6. Beale function value in its global minimum according to GA with optimization parameters stated in Table C.4.

Loop number and population size are defined according to the accuracy needed for results of optimization, considering time consumption for each run of optimization. By increasing loop number accuracy of results increases but for increasing the loop number by 1000, the run time for one run optimization with population size of 2000 increases 20 by seconds. Optimization with GA parameters presented in table 6 results in percent of standard deviation 10%.

Appendix C. 3. Optimization of Easom function

Another challenging optimization problem is defining global minimum of Easom function. This is a two variable function with several local minimums. The graph for this function shows that the global minimum searcher needs to completely cover the domain to not be trapped in local minimums. The search domain for Easom function is one order of magnitude bigger than Beale and booth functions. It is important to test the GA in big search domains, because of the big search domain range for Z_0 for optimization of PDLC films; one should make sure that GA will be able to find the global optimum of Easom function. Figure C.7 shows Easom function.

$$\text{Easom function} = -\cos(x_1) \cos(x_2) \exp(-(x_1 - \pi)^2 - (x_2 - \pi)^2) \quad (\text{C.3})$$

Variables; x_1, x_2

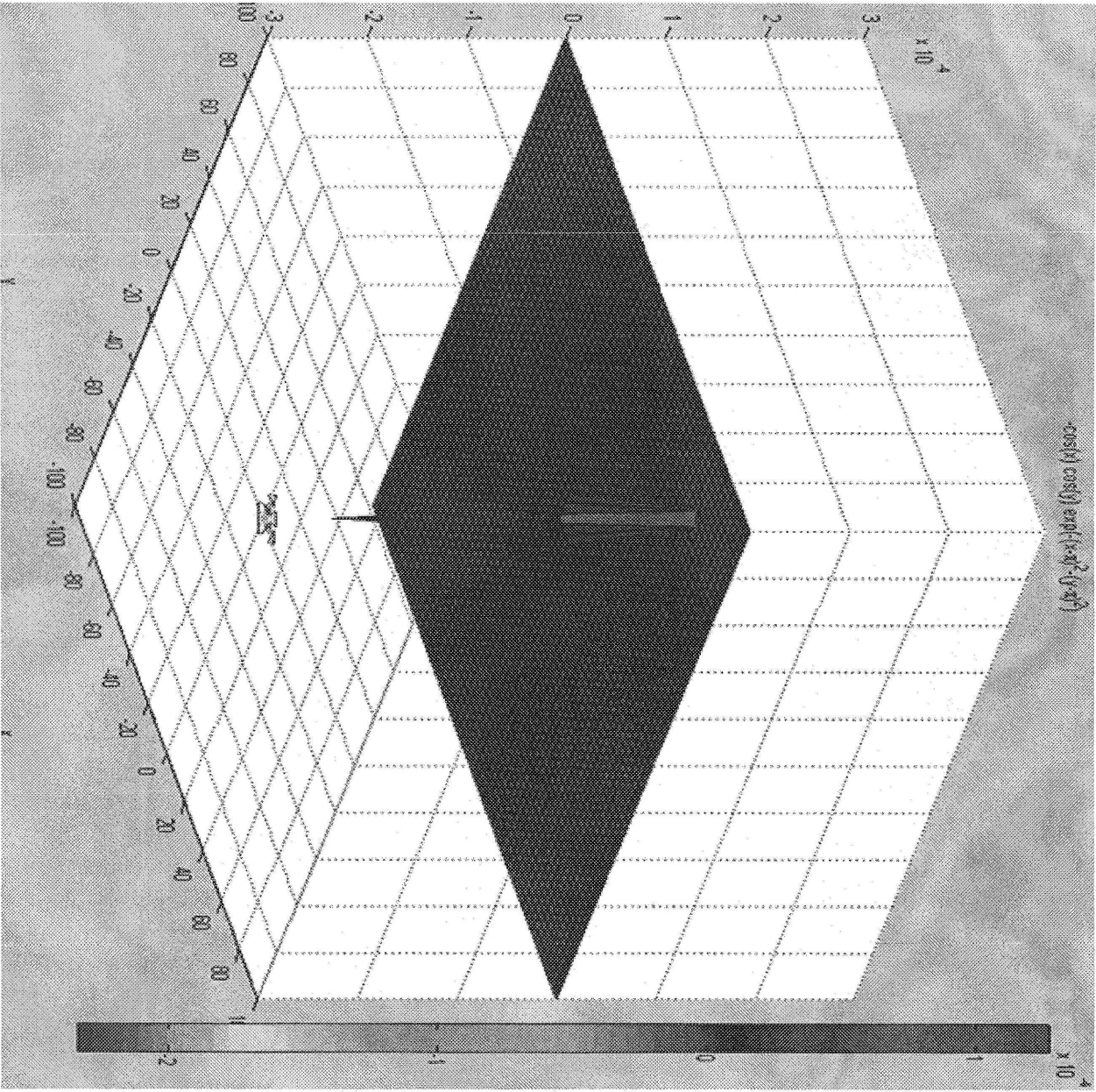


Figure C.7. Easom function with its global minima.

Specifications of Easom function are presented in Table C.5.

Table C.5. Specifications of Easom function

Easom function	
Number of variables	2
Search domain	$-100 \leq x_i \leq 100, i = 1,2$
Number of local minima	Several local minima
The global minimum	$x^{min} = (\pi, \pi)$
Objective function value in global minimum	$f(x^{min}) = -1.$

Loop number and population size for solving Easom function is defined according to the accuracy and run time, too. The range for testing loop number is 500 to 5000, where the population size is fixed on 1000. Figure C.8 shows the loop number sensitivity of Easom function. In Figure C.9 effect of population size is studied on optimization results for solving Easom function. Loop number is fixed on 3000, and the population size is changing from 100 to 2000. Results are presented in Figure C.10.

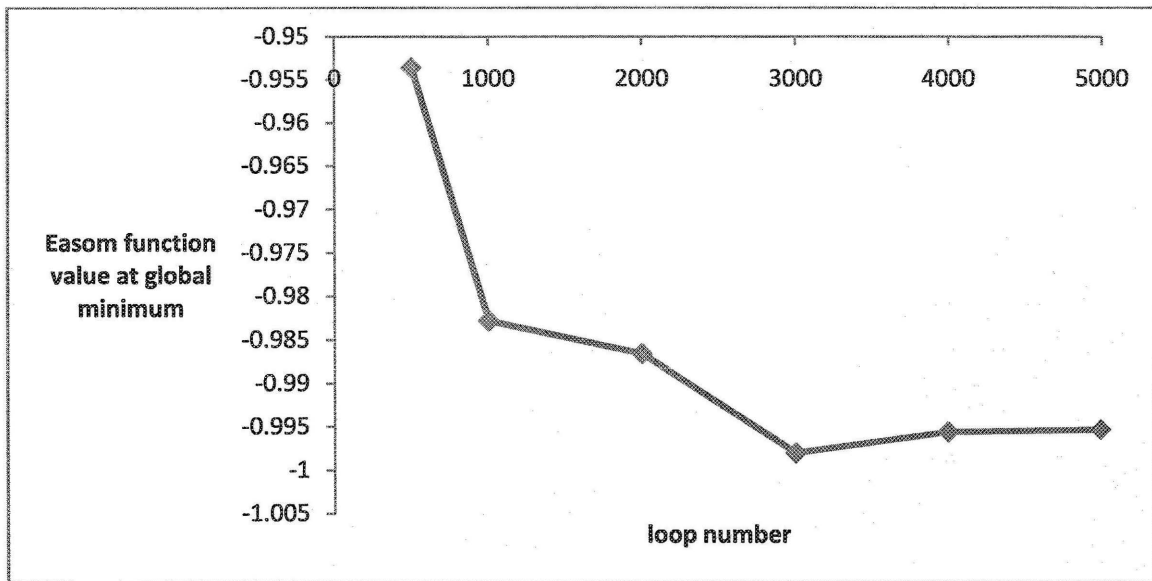


Figure C.8. Effect of loop number on accuracy of results. Value of Easom function in its global minimum is -1. Results show that by increasing loop number accuracy of results increase, and function value in its global minimum gets close to -1.

GA parameters are presented in Table C. 6. Results of optimization of Easom function with over 70 runs of GA are presented in Fig. C.11. According to Figure C.8 loop number of 3000 is chosen for optimization.

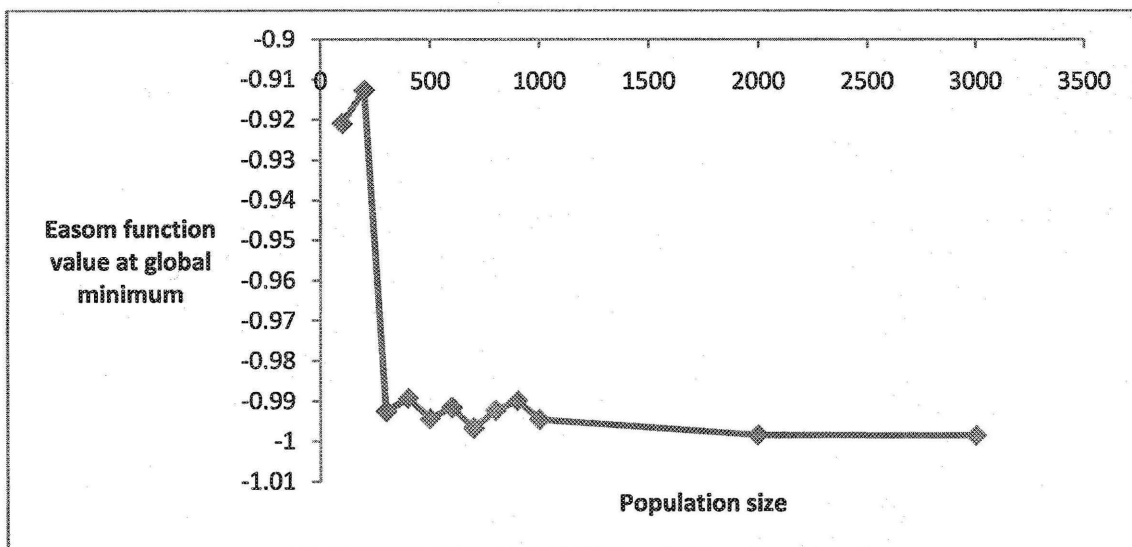


Figure C.9. Effect of population size on accuracy of optimization results. Analytical value for optimum function value at global optimum is -1.

Table C.6. Parameters for GA in solving Easom function.

Genetic algorithm	
Population	1000
Loops	3000
Gene size	15 bits
No. variables	2
Cross over rate	80%
Mutation rate	5%
Fitness function	$1/(1 + \text{Easom function})$
Seed number generator	Time of computer
No. Iteration	70
Standard deviation	0.005

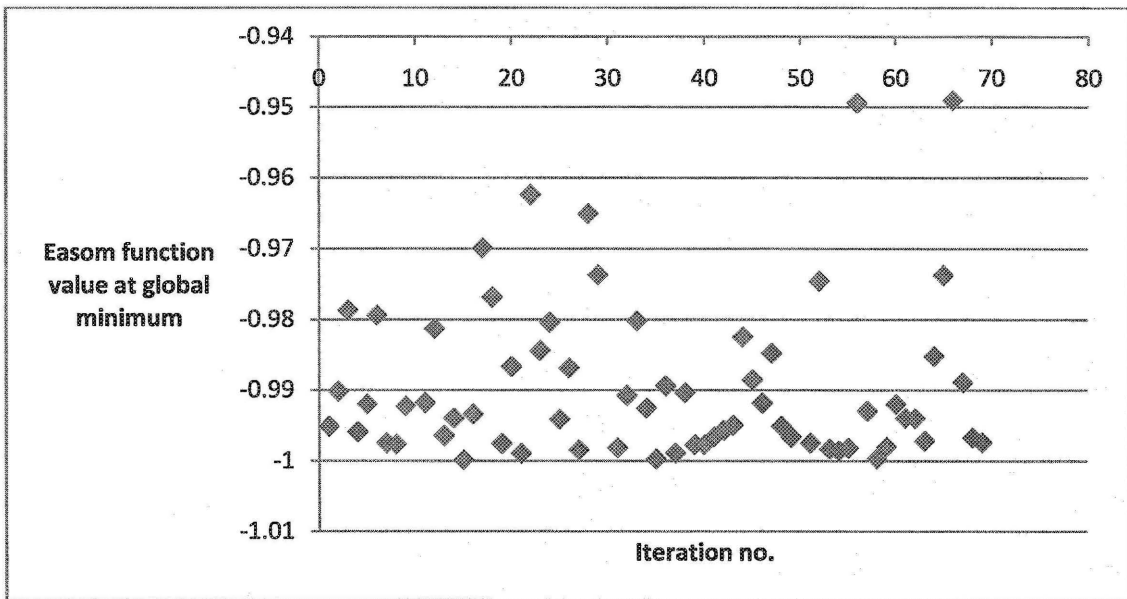


Figure C.11. Easom function value at global minimum for 70 iterations. Loop number 3000, and population size 1000. The analytical value of function at global minimum is -1.

References

- [1] Collings, P. J., **1990**, *Liquid Crystals: Natures delicate phase of matter*, (Princeton University Press)
- [2] <http://plc.cwru.edu/tutorial/enhanced/files/pdlc/intro/intro.htm>
- [3] Drzaic, P. S. **1988**, Reorientation Dynamics of Polymer Dispersed Nematic Liquid Crystal Films, *Liquid Crystals*, 3, 1543.
- [4] Drzaic, P. S. & Muller. A., **1989**, Droplet Shape and Reorientation Fields in Nematic Droplet/Polymer Films *Liquid Crystals*, 5, 1467.
- [5] Kim, H.R., Jung, J. W., Lee, Y. J & Kim, H. J., **2006**, Liquid crystal Alignment with a Molecular Template of Imprinted Polymer Layer during Phase Separation *Applied Physics Letters*, 88, 113504.
- [6] Wu. B-G., West, J. L., & Doane, J. W., **1987**, Angular Discrimination of Light Transmission through Polymer Dispersed Liquid Crystal Films *Journal of Applied Physics*, 62, 3925.
- [7] www.xixiglass.com/images/003.png
- [8] Doane, J. W. **2006**, PDLC Shutters: where has this technology gone? *Liquid crystals*, 33, 1313.
- [9] Rudhardt, D, Fernandez- Nieves. A. Link, D.R D & Weitz, D. A. **2003**, Phase Switching of Ordered Arrays of Liquid Crystal Emulsions *Physical Review Letters*, 82, No. 16.

- [10] Chan, P. K., **1999**, Computer Simulation of Elongated Bipolar Nematic Droplets, I. External Field Aligned Parallel to the Droplet axis of Symmetry, *Liquid Crystals*, 26, 1777.
- [11] Chan, P. K, Lee, K. W. D. & Tran, L. T **2001**, The Effect of Elongated Nematic Bipolar Orientation on the Performance of Polymer-Dispersed Liquid Crystal Films, *Computational Materials Science*, 21, 329.
- [12] Fergason, J. L., **1984**, Encapsulated Liquid Crystal and Method *U.S. Patent* 4,435,047.
- [13] Heilmeyer, G. H., **1976**, Liquid Crystal Displays: An Experiment in Interdisciplinary Research that Work, *IEEE Transactions on Electron Devices*, 23, 780.
- [14] Doane, J. W. & Zumer, S., **1986**, Light Scattering from a small Nematic Droplet, *Applied Physics Letters*, 48, 269.
- [15] Aphonin, O. A., Panina. YU. V., Pradin. A. B. & Yakovlev. D. A., **1993**, Optical Properties of Stretched Polymer Dispersed Liquid Crystal Films, *Liquid Crystals*, 15, 395.
- [16] Zhao, Y, Bai, S. Banh, T. N. & Brazeau, J **2000**, Orientation and Anchoring Effects in Stretched Polymer Dispersed Nematic Liquid Crystals, *Liquid Crystals* 27, 118
- [17] Amimori, I., Priezjev, N.V. Pelcovits, R. A. & Crawford, G. P **2003**, Opt mechanical Properties of Stretched Polymer Dispersed Liquid Crystal Films for Scattering Polarizer Applications, *Journal of Applied Physics*, 93, 6.
- [18] Higgins, D. A, Hall. J. E & Xie, A., **2005**, Optical Microscopy Studies of Dynamics within Individual Polymer-Dispersed Liquid Crystal Droplet, *Accounts of Chemical Research*, 38, 137.

- [19] Xie, A. & Higgins, D. A., **2004**, Electric-Field-Induced Dynamics in Radial Liquid Crystal Droplets Studied by Multiphoton-Excited Fluorescence Microscopy: Interfacial Effects and Metastable Configurations, *Applied Physics Letters*, 84, 4014.
- [20] Leslie, F. L. **1971**, Continuum theory of Liquid Crystals, *Rheologica Acta*.10, 91.
- [21] Ericksen, J. L. **1961**, Poiseuille Flow of Certain Anisotropic Fluids, Transaction of Society of Rheology, 5, 23.
- [22] Baleo, J.N., Vincent, M., Navard, P., & Demay. Y. **1992**, Finite Element Simulation of Flow and Director Orientation of Viscous Anisotropic Fluids in Complex 2D Geometries, Journal of rheology, 36, 663.
- [23] Han, W. H. & Rey, A. D, **1993**, Stationary Bifurcations and Tricriticality in a Creeping Nematic Polymer Flow *Journal of Non-Newtonian Fluid Mechanics*, 50, 1.
- [24] Chan, P. K. & Rey, A. D. **1997**, Simulation of Reorientation Dynamics in Bipolar Nematic Droplets, *Liquid Crystals*, 23, 677.
- [25] Gomes, A. E. & Polimeno, A, **2003**, Time Evolution of Director Patterns in Rotating Nematic Samples *Molecular Crystals & Liquid Crystal.*, 395,295.
- [26] Polimeno, A, Orian, L. Martins, A. F. & Gomes, A. E, **2000**, Simulations of Flow-Induced Director Structures in Nematic Liquid Crystals through Leslie-Ericksen Equations. I. Computational Methodology in Two Dimensions *Physical Review E Stat*, 62, 2288.
- [27] Chan, P. K. **2001**, Computer simulation of elongated bipolar nematic droplets, II.External field aligned normal to the droplet axis of symmetry, *Liquid Crystals* 28, No. 2, 207.

- [28] Mirantsev, L.V & Romano, S. **2006**, Molecular Dynamics Simulation of Polymer Dispersed Liquid Crystal Droplets under Competing Boundary Conditions, *Liquid Crystals*, 33, No.2.
- [29] Prishchepa, O. O, Shabanov, A.V. & Zyryanov, V. YA, **2006**, Director Configurations in Nematic Droplets with Inhomogeneous Boundary Conditions, *Physical Review E*, 72, 31712.
- [30] Hirai, Y. Niiyama, S. Kumai, H. & Gunjima, T. **1990**, Phase Diagram and Phase Separation in LC/Prepolymer Mixture, *Proc. SPIE*, 1257, 2.
- [31] Drzaic, P. **2006**, Putting Liquid Crystal Droplets to Work: a Short History of Polymer Dispersed Liquid Crystals, *Liquid Crystals*, 33, 1281.
- [32] Wu, B-G. Erdmann, J.H. & Doane, J.W. **2006** . Response times and voltages for PDLC light shutters, *Liquid Crystals*, 33, 1315.
- [33] De Gennes, P.G., Prost, J. **1993**, *The physics of Liquid Crystal*, 2nd edition, Clarendon Press, Oxford.
- [34] Haller, I. and Litster, J. D., **1970**, Temperature Dependence of Normal Modes in a Nematic Liquid Crystal, *Physical Review Letters*, 25, 1550.
- [35] Chapra, S. C., Canale, R. P., **2001**, *Numerical Methods for Engineers*, 4th edition, McGraw-Hill College.
- [36] Drzaic, P. S., **1995**, *Liquid crystal dispersions*, World Scientific.
- [37] Thompson, E.G. **2004**, *Introduction to the Finite Element Method: Theory, Programming and Applications*, I. Wiley & Sons.

[38] Deb, K. 2002, *Optimization for Engineering Design, Algorithms and Examples*, Prentice Hall of India.

[39] Goldberg, D. E., 1989, *Genetic Algorithms in Search, Optimization, and Machine Learning*. Reading, Mss.: Addison Wesley.

Dr. K. Deb